Genetically encoded lipid–polypeptide hybrid biomaterials that exhibit temperature-triggered hierarchical self-assembly

Davoud Mozhdehi[1,2 †], Kelli M. Luginbuhl[1,2 †], Joseph R. Simon[1,2], Michael Dzuricky[1,2], Rüdiger Berger[3], H. Samet Varol[4], Fred C. Huang[2], Kristen L. Buehne[2], Nick R. Mayne[2], Isaac Weitzhandler[1,2], Mischa Bonn[4], Sapun H. Parekh[4], and Ashutosh Chilkoti[1,2] *

[1] NSF Research Triangle Materials Research Science and Engineering Center, Department of Biomedical Engineering, Duke University, Durham, NC, 27708, USA

[2] Department of Biomedical Engineering, Duke University, Durham, NC, 27708, USA

[3] Physics at Interfaces, Max Planck Institute for Polymer Research, Mainz, Ackermannweg 10, 55128 Mainz, Germany

[4] Department of Molecular Spectroscopy, Max Planck Institute for Polymer Research, Ackermannweg 10, 55128 Mainz, Germany

Supplementary Information

Table of contents

1. Materials

The pETDuet-1 vector was purchased from EMD Millipore (Billerica, MA). All the restriction enzymes, ligase, and corresponding buffers were purchased from New England Biolabs (Ipswich, MA). Chemically competent Eb5alpha and BL21(DE3) cells were purchased from Edge Bio (Gaithersburg, MD). DNA extraction and purification kits were purchased from Qiagen (Valencia, CA). Terrific broth medium (TB) was purchased from Amresco (Solon, OH). Isopropyl β-D-1-thiogalactopyranoside (IPTG) was purchased from Bioline USA (Boston, MA). Myristic acid, N,N-diisopropylethylamine (DIPEA), 4-methylmorpholine, triisopropylsilane, alpha-cyano-4-hydroxycinnamic acid, Benzotriazol-1-yloxy)tris(dimethylamino)phosphonium hexa-fluorophosphate (BOP reagent), and trifluoroacetic acid (TFA) were purchased from Sigma-Aldrich (St. Louis, MO). SnakeSkin™ Dialysis Tubing featuring 3.5K nominal molecular weight cut off (MWCO), mass spectroscopy grade Pierce™ trypsin protease, Alexa Fluor® 488 NHS ester, Alexa Fluor® 488 cadaverine, and anhydrous dimethyl sulfoxide (DMSO) were purchased from Thermo Fisher Scientific (Waltham, MA). Rink amide resin (200-400 mesh, 0.6 meq/g), Fmoc-protected amino acids, O-benzotriazole-N,N,N',N'-tetramethyluronium hexafluoro-phosphate (HBTU), and O-(6-Chlorobenzotriazol-1-yl)-N,N,N′,N′-tetramethyl-uronium hexafluoro-phosphate (HCTU) were purchased from Chem-Impex (Wood Dale, IL). Diethyl ether, dichloromethane (DCM), and high performance liquid chromatography-(HPLC) grade acetonitrile were purchased from VWR International (Radnor, Pennsylvania) and were used as received without further purification. Anhydrous dimethylformamide (DMF) was purchased from EMD Millipore and was further dried over t.h.e.® Desiccant (EMD Millipore) before use. Deionized water was obtained from a Milli-Q® system (Thermo Scientific, CA).

ABIL® EM 90 and TEGOSOFT® DEC surfactants were purchased from Evonik Industries (Essen, Germany). Mineral oil was purchased from Sigma-Aldrich (St. Louis, MO). A single emulsion droplet chip was purchased from Dolomite Microfluidics (Royston, United Kingdom). Syringe pumps were purchased from Chemyx Inc. (Stafford, TX).

2. Sequence Design

2.1 Recognition sequence

In the design of our NMT recognition sequences, we have been inspired by the rich universe of previous studies on peptide amphiphiles according to principles discussed in the paper and expanded in this section. To check the feasibility of myristoylation, we used an online myristoylation predictor.[1][*] The sequences and the predictor score are summarized in the Supplementary Table 1. We did not observe any myristoylation for the last recognition sequence, GVEVERGGSGGSGGS, consistent with the predictor score (data not shown).

Supplementary Table 1. Queries and online myristoylation predictor scores for various sequences in this study.

Recognition Sequence	Query	NMT - The MYR Predictor Score	Inspired by reference
B_1	GAGASRGGSG GSGVGVPGVG VP	2.183 (Reliable site)	
B_2	GAGAGAYRGG SGGSGGSGVG VPGVGVP	-1.045 (Twilight zone, Likely site)	2
B_3	GLSLSRGGSG GSGVGVPGVG VP	1.407 (reliable site)	3
	GVEVERGGSG GSGGSGVGVP GVGVP	-5.095 (no site for myristoylation)	4

As shown in the Supplementary Table 1, three out of four designed recognition sequences were myristoylated in our system. In our experiments, the MYR predictor appeared to be a reliable indicator of myristoylation for de novo designed sequences.

2.2 β-sheet propensity of PA-domain

We have used two beta sheet propensity scales developed by Kim[5] and Regan[6] (Supplementary Table 2). We are mindful that beta sheet propensities are context-dependent[7] but in our system, we have used these relative propensities to score our recognition sequences based on their propensity to form β-sheets ($B_1 < B_2 < B_3$) by comparing the first 8 amino acids, where the sequences is divergent. We have used this rough estimate also as an indirect surrogate for the stability of PA-domains. We point out that this treatment ignores secondary interactions such as the possible hydrogen bonds between the serine side chains.

---

[*] The predictor is accessible at http://mendel.imp.ac.at/myristate/SUPLpredictor.htm

Supplementary Table 2. Experimentally observed thermodynamic scales for β-sheet forming tendencies of amino acids in the FAME sequence from references 5 and 6.

Amino Acid	$\Delta\Delta G^{5,*}$ (kcal/mol)	$\Delta\Delta G^{6}$ (kcal/mol)
Gly	1.2	1.21
Ala	0	0
Leu	-0.51	-0.45
Ser	-0.70	-0.87
Tyr	-0.96	-1.63
Arg	-0.45	-0.40
Val	-0.82	-0.94
Pro	>3	Not determined

 * For consistency between two scales, we have reported the $(-\Delta\Delta G)$ reported in reference 5. With alanine chosen as the reference, the more negative $\Delta\Delta G$ values imply higher preference for β-sheet formation.

2.3 ELP domain

Our preliminary work demonstrated that myristoylation reduces the transition temperature (T_t) of ELPs by ~ 15 °C. Based on our experience in the lab and previously developed unified model linking T_t to the length and composition of ELPs[8], we have chosen the length of the ELP with the following two considerations: 1) we aimed to maintain the transition temperature of FAMEs approximately around 20-25 °C and thus aimed to choose ELP with original T_t of ~ 40 °C, (GVGVP)$_{40}$ has a T_t of ~ 39 °C at the concentration of 100 μM. 2) We also aimed to select an ELP segment as to avoid coacervation during the expression inside *E. coli*. Initially, we hypothesized that coacervation of the ELP may preclude the *in situ* enzymatic modification. We have not tested this hypothesis explicitly, but it is worth mentioning that we have been able to myristoylated more hydrophilic ELPs with up to120 pentameric repeats (results will be reported elsewhere).

3. Gene Synthesis
3.1 Construction of the Expression Vector
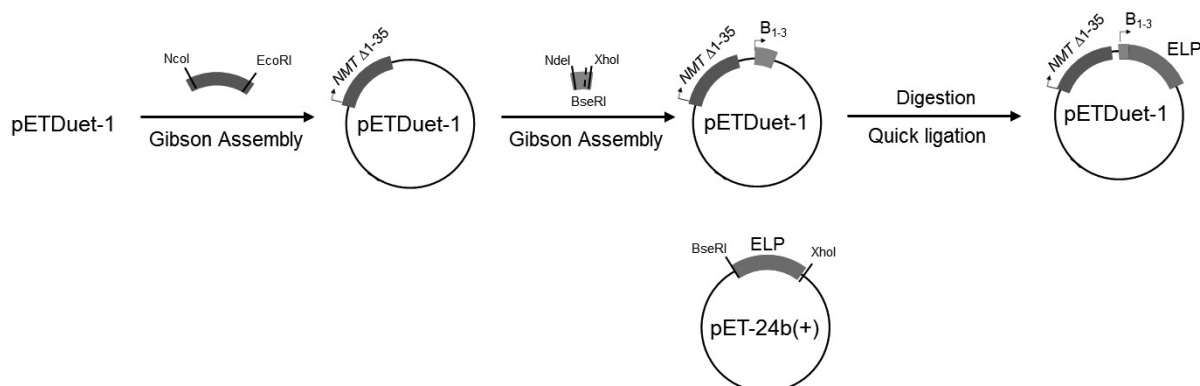
Supplementary Figure 1. Schematic of the process used to construct the dual expression vector used in the study.

To generate a single vector dual expression system, we purchased pETDuet-1 DNA from EMD Millipore. This vector contains an ampicillin resistance gene and two multiple cloning sites (MCS), each of which is preceded by its own T7 promoter, lac operator, and ribosomal binding site. The following codon optimized double stranded genes were purchased from Integrated DNA Technologies and coded for an MGSSHHHHHH leader, followed by residues 36 to 455 of the *S. cerevisiae* NMT enzyme (Swiss-Prot accession number P14743). This cDNA (shown in green) was then flanked on each end by a 40-80 bp segment that corresponded to the pETDuet-1 sequences upstream and downstream of the MCS 1 (shown in black in the gene sequence below) in addition to cleavage sites for NcoI and EcoRI (underlined). After cutting and gel purifying pETDuet-1 DNA with NcoI and EcoRI-HF, the NMT gene was inserted into MCS 1 using the Gibson Assembly® Master Mix (New England Biolabs) according to the manufacturer's instructions. Ligated DNA (3 µL) was transformed into EB5alpha (25 µL) competent cells (EdgeBio) and spread onto agar plates containing 100 µg/mL ampicillin. Positive clones were identified with Sanger sequencing (Eton Biosciences) using the universal T7 Promoter primer.

5′-CAATGGTATATCTTCCGGGCGCTATCATGCCATACCTTTTTATA<u>CCATGGG</u>CAGCA
GCCATCACCATCATCACCACAAAGACCACAAATTTTGGCGTACCCAGCCGGTTAAA
GATTTTGATGAAAAAGTTGTTGAAGAAGGTCCGATCGACAAACCGAAAACACCGGA
AGATATTAGCGATAAACCGCTGCCGCTGCTGAGCAGCTTTGAATGGTGTAGCATTGA
TGTGGACAACAAAAAACAGCTGGAAGATGTTTTTGTGCTGCTGAACGAAAACTATG
TGGAAGATCGTGATGCAGGTTTTCGCTTCAATTATACCAAAGAGTTTTTCAACTGGG
CACTGAAAAGTCCGGGTTGGAAAAAAGATTGGCATATTGGTGTTCGTGTGAAAGAA

ACCCAGAAACTGGTTGCATTTATTAGCGCAATTCCGGTTACCCTGGGTGTGCGTGGT
AAACAGGTTCCGAGCGTTGAAATTAACTTTCTGTGTGTTCATAAACAGCTGCGTAGC
AAACGTCTGACACCGGTTCTGATTAAAGAAATCACCCGTCGTGTGAACAAATGCGAT
ATTTGGCATGCACTGTATACCGCAGGTATTGTTCTGCCTGCACCGGTTAGCACCTGTC
GTTATACCCATCGTCCGCTGAACTGGAAAAAACTGTATGAAGTTGATTTCACCGGTC
TGCCGGATGGTCATACCGAAGAAGATATGATTGCAGAAATGCACTGCCTGCAAAA
ACCAAAACCGCAGGTCTGCGTAAACTGAAAAAAGAGGACATCGATCAGGTCTTTGA
GCTGTTTAAACGTTATCAGAGCCGCTTTGAACTGATCCAGATTTTTACCAAAGAAGA
GTTCGAGCACAACTTTATTGGTGAAGAAAGCCTGCCGCTGGATAAACAGGTGATTTT
TAGCTATGTTGTTGAACAGCCGGATGGCAAAATTACCGATTTTTTCAGCTTTTATAGC
CTGCCGTTTACCATTCTGAACAACACCAAATACAAAGACCTGGGCATTGGCTATCTG
TATTATTACGCAACCGATGCCGATTTCCAGTTTAAAGATCGTTTTGATCCGAAAGCA
ACCAAAGCCCTGAAAACCCGTCTGTGCGAACTGATTTATGATGCATGTATTCTGGCC
AAAAACGCCAACATGGATGTTTTTAATGCACTGACCAGCCAGGATAATACCCTGTTT
CTGGATGATCTGAAATTTGGTCCGGGTGATGGTTTTCTGAATTTCTACCTGTTTAACT
ATCGTGCCAAACCGATTACCGGTGGTCT<u>GAATCC</u>GGATAATAGCAATGATATTAAAC
GTCGCAGCAATGTTGGTGTGGTTATGCTGTGATAATGATAATGATCTTCTG**AATTCC**
CGTCATATCCGCTGAGCAATAACTAGCATAACCCCTTATACGTTACAT-**3′**

This NMT(+) vector was then modified with the cDNA (see below) of each of the three *de novo* designed NMT signal sequences (B$_{1-3}$) using the same Gibson Assembly method. The following genes (Integrated DNA Technologies) were ligated into MCS 2 after digesting the NMT(+) pETDuet-1 vector with NdeI and XhoI and purification of linearized vector. Importantly, these cDNA for NMT signal (recognition) sequence were designed to contain a BseRI recognition sequence which was engineered to cut directly after the peptide substrate gene. BseRI is a type IIS restriction enzyme that enables seamless cloning with our available in-house ELPs, many of which have been designed using the cloning system developed by McDaniel *et al.*[9] After Gibson Assembly, these new ligated vectors were transformed into competent cells and we identified positive clones with T7 Terminator sequencing. The recognition sequences for NdeI and XhoI enzymes are underlined in the sequences below.

NMT Recognition Sequence B$_1$: (GAGASRGGSGGS)
ATCTTAGTATATTAGTTAAGTATAAGAAGGAGATATA<u>CATATG</u>GGGGCGGGCGCAT
CTCGTGGTGGCAGTGGTGGGAGCGGcTAATGATCTCCTCTATGAGGATCCG<u>CTCGAG</u>
TCTGGTAAAGAAACCGCTGCTGCGAAATTTGAA

NMT Recognition Sequence B$_2$: (GAGAGAYRGGSGGSGGS)
CATCTTAGTATATTAGTTAAGTATAAGAAGGAGATATA<u>CATATG</u>GGGAGCGGGTGCA
GGTGCCTATAGAGGTGGGTCGGGAGGCAGTGGAGGCTCAGGCTAATGATCTCCTCA
ATGAG<u>CTCGAG</u>TCTGGTAAAGAAACCGCTGCTGCGAAATTTGAACG

NMT Recognition Sequence B₃: (GLSLSRGGSGGS)
ATCTTAGTATATTAGTTAAGTATAAGAAGGAGATATA<u>CATATG</u>GGGCTGAGCCTGTC
TCGTGGTGGCAGTGGTGGGAGCGGCTAATGATCTCCTCAATGAG<u>CTCGAG</u>TCTGGTA
AAGAAACCGCTGCTGCGAAATTTGAA

The final plasmid was constructed by digesting a plasmid containing the ELP gene and each NMT
(+) vector (now containing NMT in MCS 1 and one of the three recognition sequences in MCS 2)
with BseRI and XhoI. After gel purification, the ELP was ligated into each vector and transformed
into EB5alpha cells. After confirming positive clones with T7 Terminator sequencing, the DNA
was transformed into BL21(DE3) competent cells for expression.

3.2 Construction of Control Plasmids
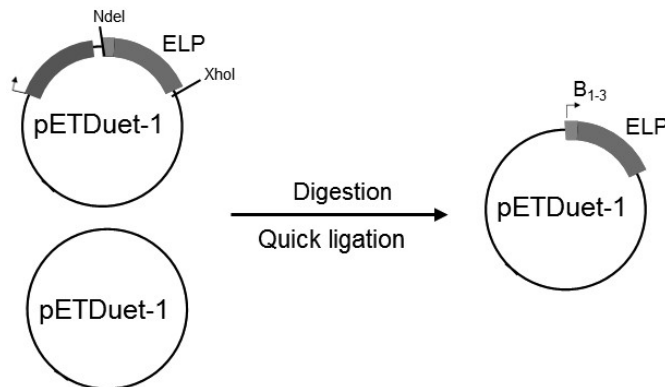
Supplementary Figure 2. Schematic of the process to prepare control plasmids.

Control plasmids without NMT were prepared for the synthesis of non-myristoylated proteins.
Briefly, empty pET-Duet-1 and plasmids containing the NMT and B₁₋₃ELP genes were digested
with NdeI and XhoI and gel purified. B₁₋₃ELP was ligated into MCS-2 of the empty pET-Duet-1
vector and transformed into EB5alpha cells. After confirming positive clones with T7 Terminator
sequencing, the DNA was transformed into BL21(DE3) competent cells for expression.

3.3 Amino Acid Sequence of Proteins

The amino acid sequences of the proteins used in this study are reported below. N-terminal
methionine is shown in italics and was removed co-translationally by methionine aminopeptidase
before modification with the myristoyl group. A lysine residue was included for fluorophore
conjugation as shown (underlined). A single tryrosine residue was encoded at the C-terminal to
assist with UV-Vis detection of the proteins.

ELP

*M*GVGVPGVGVPGVGVPGVGVPGVGVPGVGVPGVGVPGVGVPGVGVPGVGVP
GVGVPGVGVPGVGVPGVGVPGVGVPGVGVPGVGVPGVGVPGVGVPGVGVPG
VGVPGVGVPGVGVPGVGVPGVGVPGVGVPGVGVPGVGVPGVGVPGVGVPGV
GVPGVGVPGVGVPGVGVPGVGVPGVGVPGVGVPGY

B₁-ELP

*M*GAGASRGGSGGSGVGVPGVGVPGVGVPGVGVPGVGVPGVGVPGVGVPGVG
VPGVGVPGVGVPGVGVPGVGVPGVGVPGVGVPGVGVPGVGVPGVGVPGVGV
PGVGVPGVGVPGVGVPGVGVPGVGVPGVGVPGVGVPGVGVPGVGVPGVGVP
GVGVPGVGVPGVGVPGVGVPGVGVPGVGVPGVGVPGVGVPGVGVPGY

B₂-ELP

*M*GAGAGAYRGGSGGSGGSGVGVPGVGVPGVGVPGVGVPGVGVPGVGVPGVG
VPGVGVPGVGVPGVGVPGVGVPGVGVPGVGVPGVGVPGVGVPGVGVPGVGV
PGVGVPGVGVPGVGVPGVGVPGVGVPGVGVPGVGVPGVGVPGVGVPGVGVP
GVGVPGVGVPGVGVPGVGVPGVGVPGVGVPGVGVPGVGVPGVGVPGY

B₃-ELP

*M*GLSLSRGGSGGSGVGVPGVGVPGVGVPGVGVPGVGVPGVGVPGVGVPGVG
VPGVGVPGVGVPGVGVPGVGVPGVGVPGVGVPGVGVPGVGVPGVGVPGVGV
PGVGVPGVGVPGVGVPGVGVPGVGVPGVGVPGVGVPGVGVPGVGVPGVGVP
GVGVPGVGVPGVGVPGVGVPGVGVPGVGVPGVGVPGVGVPGVGVPGY

B₁-ELP-GKG

*M*GAGASRGGSGGSGVGVPGVGVPGVGVPGVGVPGVGVPGVGVPGVGVPGVG
VPGVGVPGVGVPGVGVPGVGVPGVGVPGVGVPGVGVPGVGVPGVGVPGVGV
PGVGVPGVGVPGVGVPGVGVPGVGVPGVGVPGVGVPGVGVPGVGVPGVGVP
GVGVPGVGVPGVGVPGVGVPGVGVPGVGVPGVGVPGVGVPGVGVPGG<u>K</u>GY

B₂-ELP-GKG

*M*GAGAGAYRGGSGGSGGSGVGVPGVGVPGVGVPGVGVPGVGVPGVGVPGVG
VPGVGVPGVGVPGVGVPGVGVPGVGVPGVGVPGVGVPGVGVPGVGVPGVGV
PGVGVPGVGVPGVGVPGVGVPGVGVPGVGVPGVGVPGVGVPGVGVPGVGVP
GVGVPGVGVPGVGVPGVGVPGVGVPGVGVPGVGVPGVGVPGVGVPGG<u>K</u>GY

B₃-ELP-GKG

*M*GLSLSRGGSGGSGVGVPGVGVPGVGVPGVGVPGVGVPGVGVPGVGVPGVG
VPGVGVPGVGVPGVGVPGVGVPGVGVPGVGVPGVGVPGVGVPGVGVPGVGV
PGVGVPGVGVPGVGVPGVGVPGVGVPGVGVPGVGVPGVGVPGVGVPGVGVP
GVGVPGVGVPGVGVPGVGVPGVGVPGVGVPGVGVPGVGVPGVGVPGG<u>K</u>GY

4. Expression Protocol

A single bacterial colony was selected to inoculate 50 mL of autoclaved TB medium containing 100 μg/mL ampicillin at 37 °C on an orbital shaker at 200 rpm. After 12 h, the seed culture was centrifuged at 3500 rpm and 4 °C for 15 min to harvest the cells. The *E. coli* pellet was re-suspended in 6 mL of phosphate buffer saline (PBS) solution. 1 mL of this suspension was used to inoculate 1 L of autoclaved TB media containing 100 μg/mL ampicillin. The bacteria were cultivated in an orbital shaker incubator at 37 °C at 180 rpm. After 6 h, the temperature of the incubator was reduced to 28 °C. Myristic acid was added to each flask to a final concentration of 100 μM (i.e., 1 mL of 100 mM myristic acid that had been dissolved in molecular biology grade DMSO was added to each flask). After 15 min, expression was induced by the addition of IPTG to a final concentration of 0.5 mM.

5. Protein Purification Protocol

After 18 h post-induction, the cells were harvested by centrifugation at 3500 rpm and 4 °C for 15 min. The bacterial pellet was re-suspended in PBS (5 mL PBS for each 1 L of expression culture). The cells were then lysed by two cycles of sonication at 4 °C using sequential pulses of 10 s at 85 W followed by 40 s resting-time for a total sonication period of 90 s. The lysed bacterial solution was transferred to polycarbonate centrifuge tubes and 10% w/v polyethylenimine (2 mL per every 1 L of expression culture) was added to remove the nucleic acid fragments. Each tube was vortexed several times to ensure complete mixing until a white homogeneous precipitate appeared in the entire volume of the solution. After which, the solution was centrifuged at 14 krpm and 4 °C for 15 min to separate the protein from insoluble cell debris. The clear supernatant layer was transferred to clear polycarbonate tubes and was then subjected to two rounds of inverse transition cycling (ITC). First, we triggered the phase-transition of the Fatty Acid Modified ELPs (FAMEs) or ELPs isothermally by the addition of solid NaCl. The polymer coacervates were then collected by a "hot spin" centrifugation step at 15 krpm and 35 °C for 15 min, after which the supernatant was discarded. The pellet was then re-suspended in 4 mL of deionized H_2O, and the tubes were placed in a tube rotisserie within a 4 °C refrigerator. After 1 h, the pellets were scraped with a metallic spatula to help the solubilization process. After 6 h, the mixture was centrifuged at 15 krpm and 4 °C for 15 min for a "cold spin" step, and then the pellet was discarded. The supernatant was delivered to a clean tube and was subjected to another round of ITC. For the second round of

ITC, a 5 M NaCl aqueous solution was used to trigger the phase-transition of FAMEs or ELPs isothermally. After the second "cold spin" cycle, the supernatant was collected and purified by preparative HPLC as described below to ensure purity (>95%) for the self-assembly studies.

Reverse phase HPLC (RP-HPLC) was performed on a Waters 600 HPLC system (Phenomenex Jupiter® 10 μm C18 300 Å, LC Column 250 × 21.2 mm, solvent A: H_2O + 0.1% TFA, solvent B: acetonitrile + 0.1% TFA). A sample of the protein (0.5 mL, 5 mg/mL) was injected into the HPLC system using these conditions (Supplementary Table 3) and the absorbance was monitored at 230 nm.

Supplementary Table 3. Gradient program used for preparative RP-HPLC

Time (min)	Solvent B%
0	30%
5	30%
25	90%
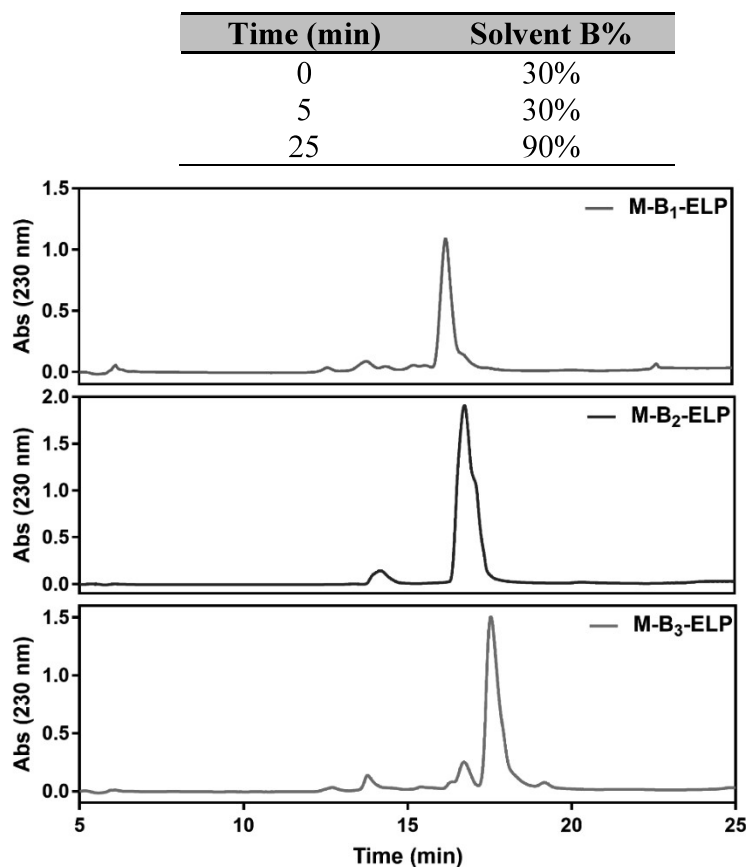
Supplementary Figure 3. RP-HPLC trace for crude FAMEs after two rounds of ITC. Phase-behavior of FAMEs allows scalable and facile purification using ITC.

The crude HPLC traces are shown in Supplementary Figure 3. Generally, two or three rounds of ITC were enough to purify FAMEs to an acceptable degree (>90%). Despite our efforts to keep the temperature below 35 °C during "hot spin", we noticed that pellet containing M-B$_2$-ELP and

M-B$_3$-ELP were noticeably stiffer than canonical ELPs. We attributed this observation to the formation of entangled network of fibers inside viscous coacervate. However, HPLC purification had an added benefit of "resetting" the self-assembly memory of the system (i.e. no fiber is observed in the lyophilized powder after HPLC). The lyophilized powder of all HPLC purified constructs exhibited similar internal structure and morphology (Section 21, Supplementary Figure 39).

Fractions corresponding to each peak were collected and analyzed using matrix-assisted laser desorption/ionization time-of-flight mass spectrometry (MALDI-TOF-MS) using an Applied Biosystems Voyager-DE™ PRO instrument according to the procedure below.

Fractions containing the desired proteins were combined and dialyzed extensively against deionized water at 4 °C using a snake skin dialysis tube with a MWCO of 3.5 kDa for 12 h. After dialysis, each sample was lyophilized (average yield 10-15 mg/L of culture for different FAMEs) and kept at -20 °C for long-term storage. The purity and identity of the constructs were assessed by sodium dodecyl sulfate polyacrylamide gel electrophoresis (SDS-PAGE), analytical HPLC, and MALDI-TOF. The N-terminal myrisotylation was further confirmed by digesting the FAME constructs with trypsin and analyzing the N-terminal peptide fragment using MALDI-TOF-MS.

6. Synthesis of Control Peptide Amphiphiles

Control peptide amphiphiles (PAs) were synthesized using standard Fmoc (9-fluorenylmethoxy-carbonyl)-based chemistry on rink amide resin using Protein Technologies PS3 automated peptide synthesizer.[10] We coupled standard Fmoc-protected amino acids using 4 equivalents of HBTU-activated amino acids in the presence of *N*-methylmorpholine in DMF for 20 min. Fmoc deprotection was achieved using 20% piperidine in DMF. Myristic acid was coupled as the last residue using a similar protocol used for coupling the canonical amino acids. After the last coupling reaction, the resin was washed twice with DMF, twice with dichloromethane, and then air-dried. Peptide cleavage and deprotection was accomplished by re-suspending the resin in 5 mL of a cleavage cocktail (95% TFA, 2.5% H$_2$O, and 2.5% triisopropylsilane) for 3 h. The resin was filtered and the cleavage cocktail was concentrated in vacuo. Peptides were precipitated in cold diethyl ether and were collected by centrifugation at 3500 rpm and 4 °C for 15 min. The pellet was washed with cold diethyl ether and air dried before storage at -20 °C. The purity and the identity

of each peptide was confirmed by liquid chromatography–mass spectrometry and MALDI-TOF-MS.

Alternatively, the control PAs could be synthesized by trypsin digestion of the corresponding FAME, similar to a method described below (see section 9.3). Briefly, to biosynthetically produce the PAs, 10 mg of the corresponding FAME (dissolved in 1 mL of digest buffer) and 1 μg of trypsin were incubated at 37 °C overnight. The PAs was collected by centrifugation and further purified by utilizing the thermally-triggered phase transition of the ELP domains and the low-solubility of PAs in water.

7. Chemical Synthesis of M-ELP

M-ELP was prepared as a control to investigate the contribution of PA-domains to the self-assembly and phase-transition of FAMEs. Due to the lack of a recognition sequence in this construct, it was not possible to prepare M-ELP through co-expression with NMT enzyme. Instead, we devised an alternative semisynthetic method to prepare this construct as shown in Supplementary Figure 4. ELP and M-ELP were studied using turbidimetry (Supplementary Figure 20 and S24), DLS (Figure 3a), CD (Supplementary Figure 26), FT-IR (Figure 3b, c), and ThT fluoresce assays (Figures 3d,e) to dissect the effect of the self-assembly domain. The combination of this data proves that the PA-domain is necessary for the control of self-assembly and macroscale morphogenesis.
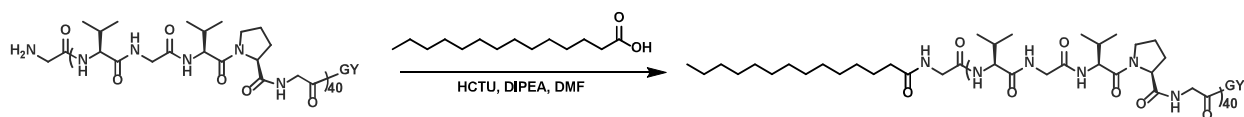
Supplementary Figure 4. Semisynthetic preparation of M-ELP.

In this procedure, myristic acid (1.0 mg, 4.4 μmol, 4.4 equiv) was dissolved in 1.0 mL DMF in a glass scintillation vial. HCTU (1.8 mg, 4.4 μmol, 4.4 equiv) and DIPEA (1.0 μL, 6.0 μmol, 6.0 equiv) were added to the vial to activate the fatty acid. After 15 min, the ELP (47 mg, 2.8 μmol, 1.0 equiv) was added to the vial and the reaction was stirred overnight. The reaction was quenched by the addition of 9 mL deionized water. The mixture was then transferred to a dialysis bag, and water soluble impurities were dialyzed against 4 L of deionized water. The M-ELP construct was then purified by RP-HPLC as described in section 5 and lyophilized (33.1 mg, 70% yield).

## 8. Fluorescent Labeling of Proteins

A lysine residue was encoded near the C-terminal of the protein to ensure that the fluorophore conjugation site was distant from the PA-domain. Labeling genetically encoded lysine was achieved using NHS-activated Alexa Fluor® 488 dye. The M-B$_{1-3}$ELP-GKG construct (25 mg, 1.4 µmol) was dissolved in anhydrous DMF (1 mL), and the labelling dye (~1 mg, 1.6 µmol, 1.1 equiv) was dissolved in anhydrous DMSO (1 mL) before use. The dye and the protein solution were mixed, followed by the addition of DIPEA (3 µL, 18 µmol, 16 equiv). After 12 h, the reaction was quenched by the addition of water (8 mL), and water-soluble impurities were subsequently removed by dialysis against 4 L of deionized water. The fluorescently labeled protein was separated from the unreacted dye using RP-HPLC by monitoring the absorbance at 230 nm and 350 nm using the protocol described in section 5. The labeling efficiency was determined by dissolving a known amount of labeled protein in water and measuring the absorbance at 494 nm (according to the manufacturer protocol, the ε_{494} of Alexa Fluor® 488 dye is 71000 cm^{-1}M^{-1}). Based on this measurement, we determined that the labeling efficiency was 42% for M-B$_1$-ELP-GKG, 37% for M-B$_2$-ELP-GKS, and 32% for M-B$_3$-ELP-GKG. For the fluorescence microscopy experiments (Sections 16 and 17), the molar ratio of the fluorescently-labeled to unlabeled FAMEs was kept at 25% by adding unlabeled FAME constructs as needed. The N-terminal amine of control ELP was labeled using a similar procedure.

A modified procedure was developed to label the C-terminal carboxylic acid of M-ELP with Alexa Fluor® 488. In this procedure, M-ELP (10 mg, 0.62 µmol, 1.0 equiv) was dissolved in 1.0 mL DMF in a glass scintillation vial. BOP reagent (0.27 mg, 0.62 µmol, 1.0 equiv) and DIPEA (1.0 µL, 6.0 µmol, 10 equiv) were added to the vial to activate the C-terminal carboxylic acid. After 15 min, the Alexa Fluor® 488 cadaverine (0.5 mg, 0.78 µmol, 1.3 equiv), dissolved in 0.5 mL of anhydrous DMSO, was added to the vial and the reaction was stirred overnight. The reaction was quenched by the addition of 9 mL deionized water. The mixture was then transferred to a dialysis bag, and water-soluble impurities were dialyzed against 4 L of deionized water. The M-ELP-AF construct was then purified by RP-HPLC as described in section 5 and lyophilized (6.0 mg, 60% yield, 34% labeling efficiency).

9. Characterization

9.1 SDS-PAGE

The purity and molecular weight of the purified proteins was characterized using a 10–20% gradient Tris-glycerol SDS-PAGE gel (Thermo Scientific, CA). The gels were negatively stained by incubation with 0.5 M $CuCl_2$ for 20 min before imaging using a BioRad Universal imager.
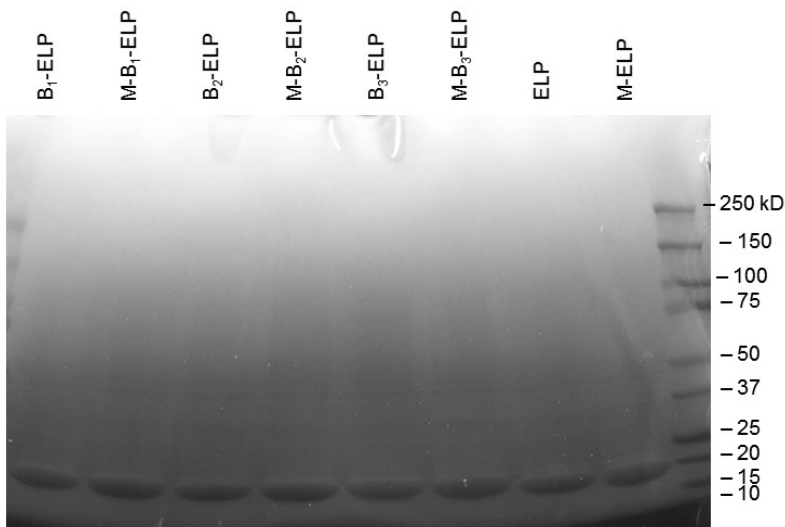
**Supplementary Figure 5. Negatively stained SDS-PAGE gel of purified constructs in this study.**

9.2 Analytical HPLC

Analytical RP-HPLC was performed on a Shimadzu instrument using a Phenomenex Jupiter® 5 µm C18 300 Å, LC Column 250 × 4.6 mm, solvent A: H_2O + 0.1% TFA, solvent B: acetonitrile + 0.1% TFA).

Supplementary Table 4. Gradient program used for analytical RP-HPLC.

Time (min)	Solvent B (%)
0	30
3	30
30	90

Constructs were dissolved in deionized water at a concentration of 70 µM. 35 µL of this solution was injected and analyzed using a photo-diode array detector to measure the absorbance at wavelengths between 190 nm and 800 nm. Representative chromatograms (at 230 nm) for each protein is displayed in Supplementary Figures 6 to 12. In all these figures, the percentage of acetonitrile (right Y axis, solvent B%) in the eluent is shown with a solid grey line. Small peaks that are visible before 5 min correspond to system peaks arising from the difference between the sample diluent (i.e., deionized water) and the mobile phase.
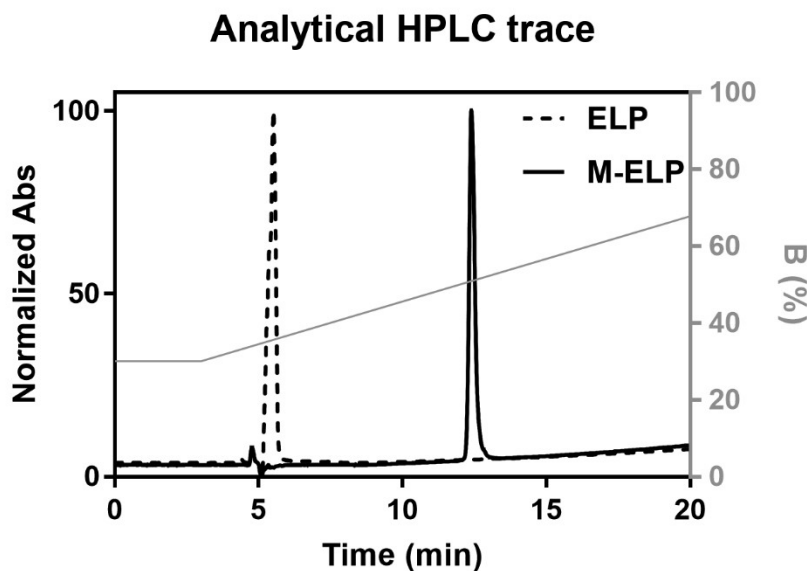
Supplementary Figure 6. Analytical RP-HPLC trace for ELP (dashed black line) and M-ELP (solid black line).
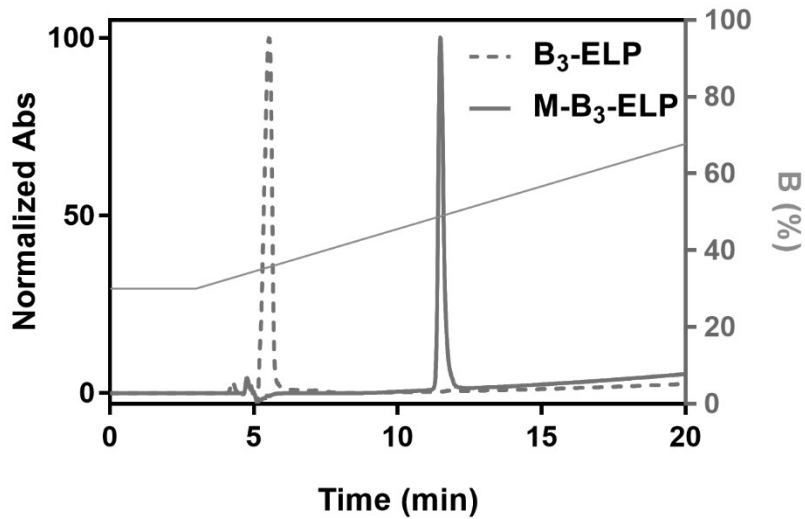
Analytical HPLC trace
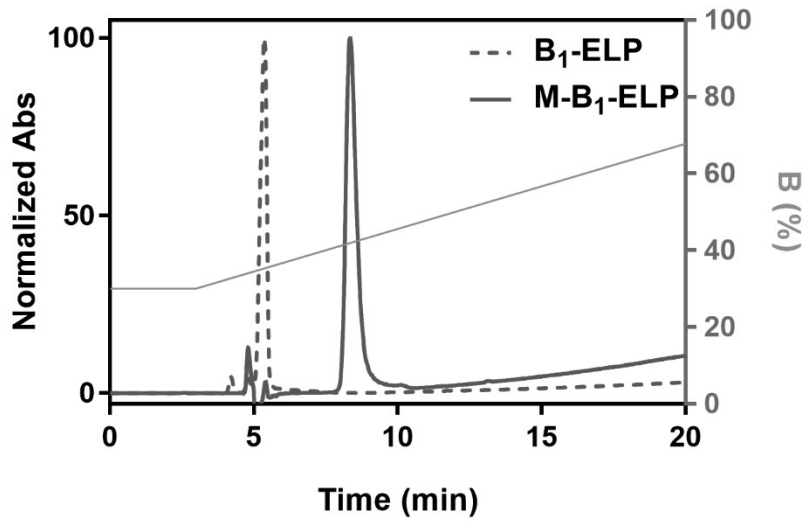
Supplementary Figure 7. Analytical RP-HPLC trace for B$_1$-ELP (dashed green line) and M-B$_1$-ELP (solid green line).
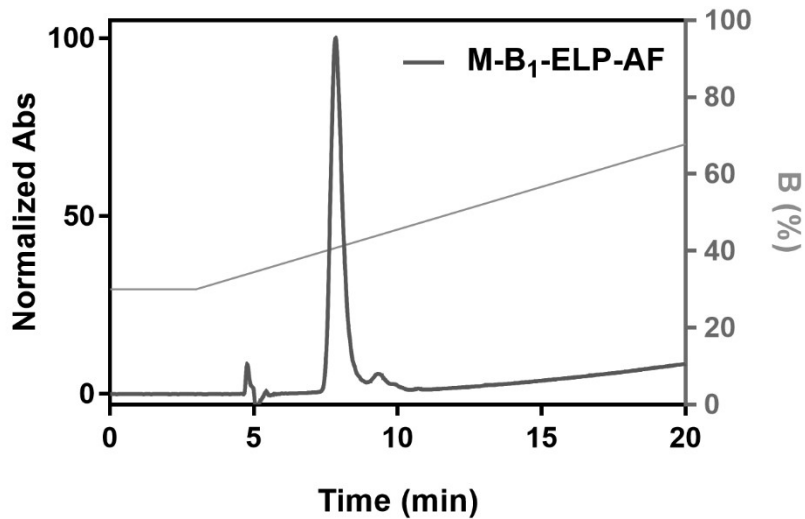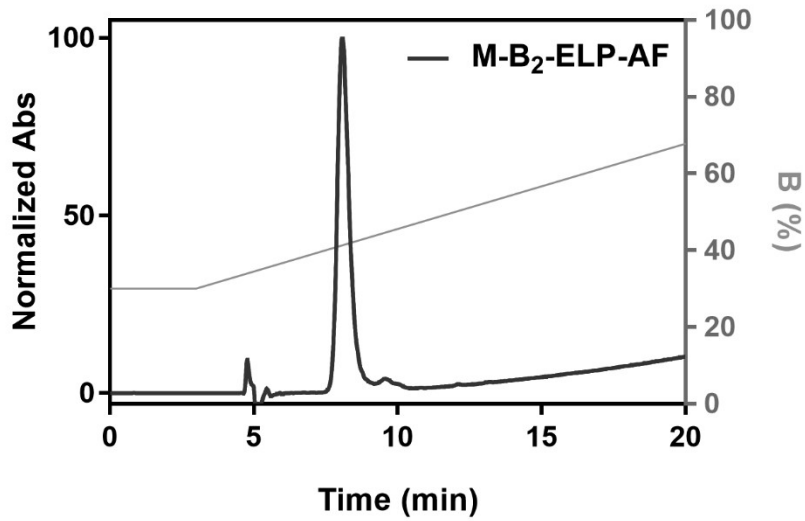

Analytical HPLC trace
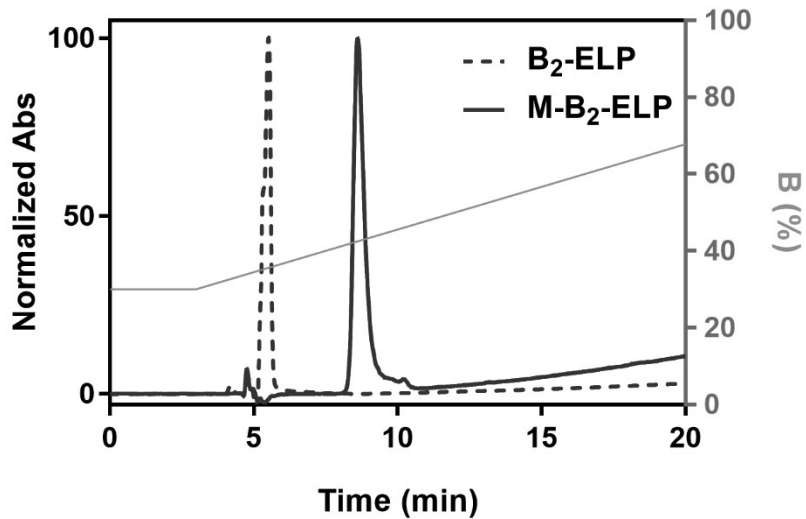
Supplementary Figure 8. Analytical RP-HPLC trace for B$_2$-ELP (dashed blue line) and M-B$_2$-ELP (solid blue line).

Supplementary Figure 9. Analytical RP-HPLC trace for B$_3$-ELP (dashed red line) and M-B$_3$-ELP (solid red line).
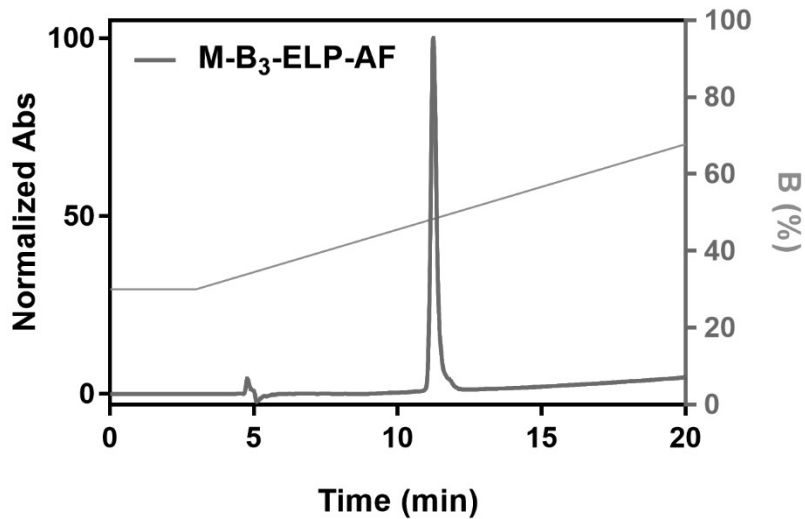

Supplementary Figure 10. Analytical RP-HPLC trace for M-B$_1$-ELP-GKG labeled with Alexa Fluor® 488 dye (AF).

Analytical HPLC trace

Supplementary Figure 11. Analytical RP-HPLC trace for M-B$_2$-ELP-GKG labeled with Alexa Fluor® 488 dye (AF).

Analytical HPLC trace

Supplementary Figure 12. Analytical RP-HPLC trace for M-B$_3$-ELP-GKG labelled with Alexa Fluor® 488 dye (AF).

9.3 Trypsin Digestion of Proteins

Trypsin digestion was conducted according to the manufacturer's protocol. Briefly, 10 μL of 50 mM ammonium bicarbonate buffer (pH = 7.8) was added to an Eppendorf tube. 9 μL of each construct was added to this reaction tube for a final concentration of 100 μM. To this mixture, 1 μL trypsin (reconstituted as1 μg/μL trypsin in 50 mM acetic acid) was added and the reaction mixture was incubated at 37 °C. After 2 h, the N-terminal fragment peptide was analyzed by MALDI-TOF-MS.

9.4 MALDI-TOF-MS

Samples for MALDI-TOF-MS analysis were prepared by mixing 10 μL of each HPLC fraction with 10 μL of the sinapinic acid (SA) matrix (a saturated solution was prepared by suspending 10 mg of SA in 700 μL H_2O + 0.1% TFA and 300 μL acetonitrile + 0.1% TFA). Afterward, 3 μL of this mixture was deposited onto a sample plate and dried in air at room temperature. All spectra with an acceptable signal-to-noise (S/N) ratio (>10) were calibrated against an aldolase standard (Sigma Aldrich, M_w = 39,211.28 Da). The following instrument parameters were optimized empirically to maximize the S/N ratio: accelerating voltage = 25 kv; grid voltage = 90%; guide wire = 0.15%; extraction delay time = 750 ns; acquisition range: 10,000-60,000 Da; low mass gate = 5000 Da; number of laser shots = 75/spectrum; laser intensity = 3000; bin size = 4 ns.

We used α-cyano-4-hydroxycinnamic acid as a matrix for analysis of the N-terminal peptide fragments and canonical peptide amphiphiles. All spectra were calibrated against adrenocorticotropic hormone fragment 18-39 (Sigma Aldrich, M_w = 2,464.1989). The following instrument parameters were optimized empirically to maximize the S/N ratio: accelerating voltage = 20 kv; grid voltage = 73.5%; guide wire = 0.005%; extraction delay time = 90 ns; acquisition range: 500-400 Da; low mass gate = 500 Da; number of laser shots = 40/spectrum; laser intensity = 2000; bin size = 0.5 ns.
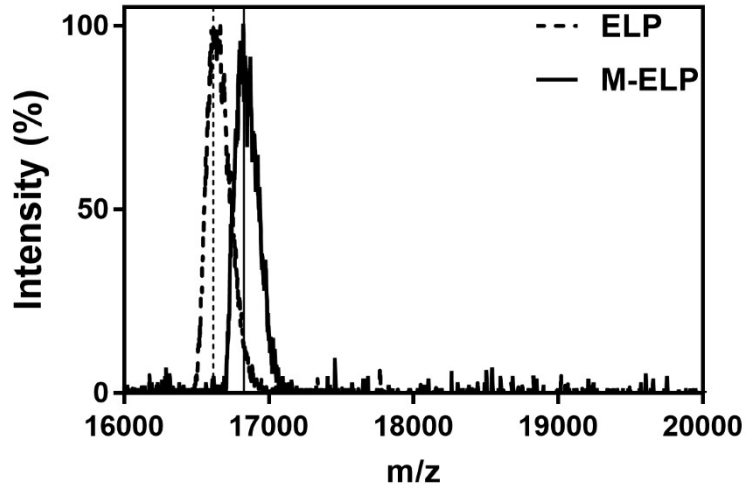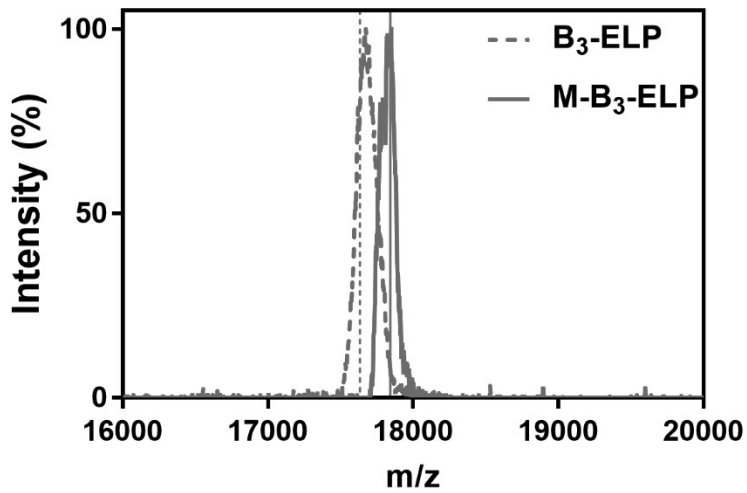
Supplementary Figure 13. MALDI-TOF-MS spectra of ELP (dashed black curve) and M-ELP (solid black curve). Vertical lines represent the theoretical M_w of each construct.
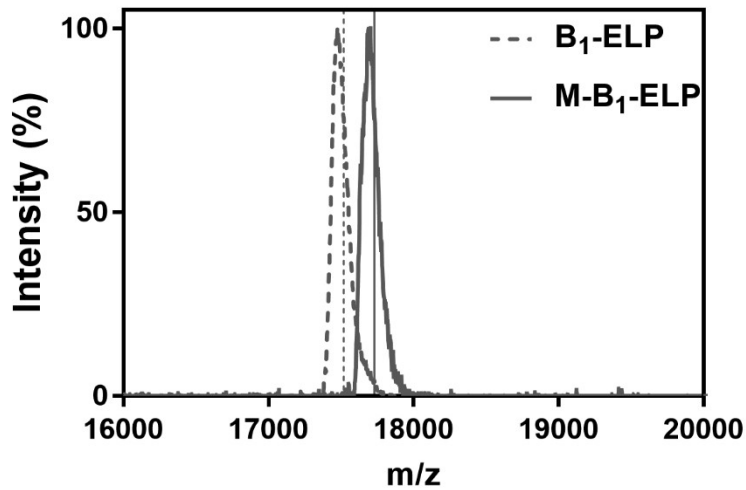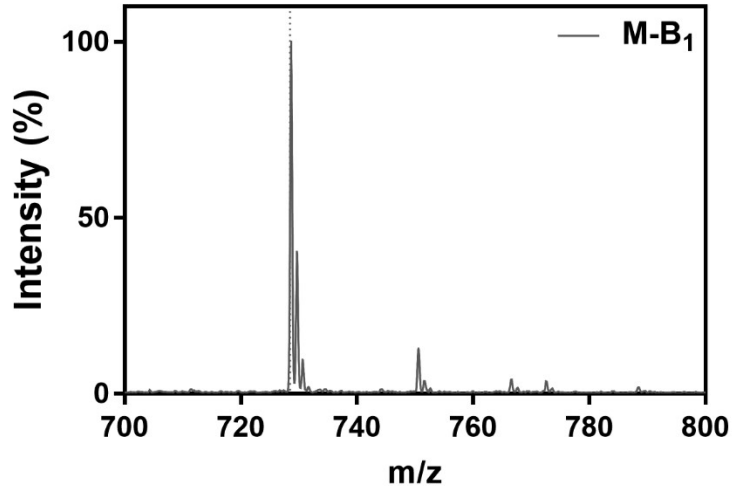

Supplementary Figure 14. MALDI-TOF-MS spectra of B_1-ELP (dashed green curve) and M-B_1-ELP (solid green curve). Vertical lines represent the theoretical M_w of each construct.
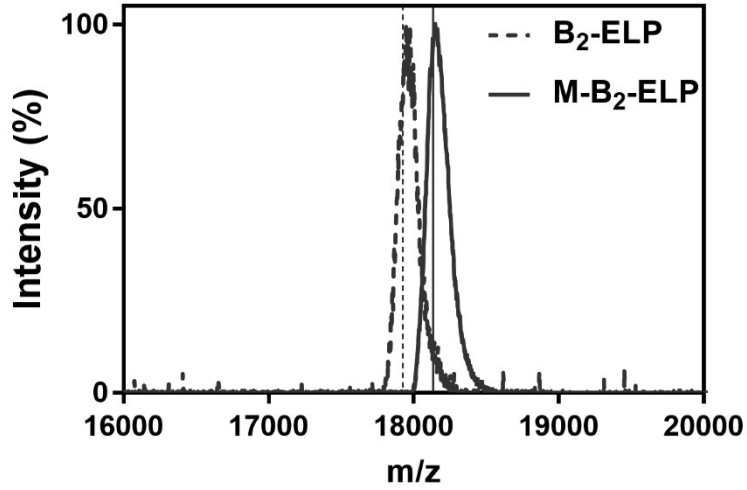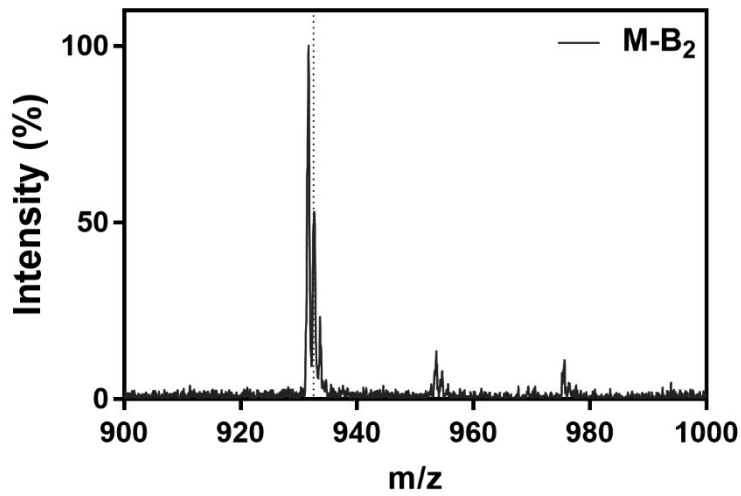
Supplementary Figure 15. MALDI-TOF-MS spectra of B2-ELP (dashed blue curve) and M-B2-ELP (solid blue curve). Vertical lines represent the theoretical M_w of each construct.

Supplementary Figure 16. MALDI-TOF-MS spectra of B3-ELP (dashed red curve) and M-B3-ELP (solid red curve). Vertical lines represent the theoretical M_w of each construct.

Supplementary Figure 17. MALDI-TOF-MS spectra of M-B₁ peptide (green) confirms N-terminal myristoylation. Vertical line represents the theoretical M_w.

Supplementary Figure 18. MALDI-TOF-MS spectra of M-B₂ peptide (blue) confirms N-terminal myristoylation. Vertical line represents the theoretical M_w.
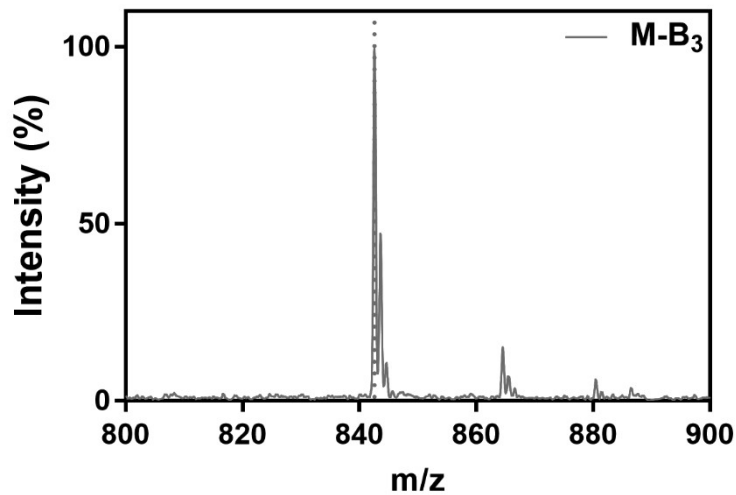
Supplementary Figure 19. MALDI-TOF-MS spectra of M-B$_3$ peptide (red) confirms N-terminal myristoylation. Vertical line represents the theoretical M$_w$.

Supplementary Table 5. Summary of MALDI-TOF-MS experiments.

	Construct	M$_W$ (Da, calculated)	m/z [M+H]$^+$ (observed)
Proteins	ELP	16617.7	16616.2
	M-ELP	16828.0	16822.9
	B$_1$-ELP	17519.6	17476.3
	M-B$_1$-ELP	17729.9	17702.6
	B$_2$-ELP	17924.9	17948.1
	M-B$_2$-ELP	18135.3	18147.2
	B$_3$-ELP	17633.7	17674.4
	M-B$_3$-ELP	17844.1	17849.0
Peptides	M-B$_1$	727.4	728.7
	M-B$_2$	931.6	931.6
	M-B$_3$	841.6	842.6

10. UV-Visible Spectroscopy

We investigated the temperature-triggered phase-transition of each construct by recording the optical density of the protein solution at 350 nm as a function of temperature, from 15 °C to 50° C (ramping at a rate of 1 °C/min) on a temperature controlled UV−Vis spectrophotometer (Cary 300 Bio, Varian Instruments, Palo Alto, CA). The transition temperature (T_t) is defined as the inflection point of the turbidity profile. Turbidity profiles for each sample were measured in PBS at three different solution concentrations between 25−100 μM.
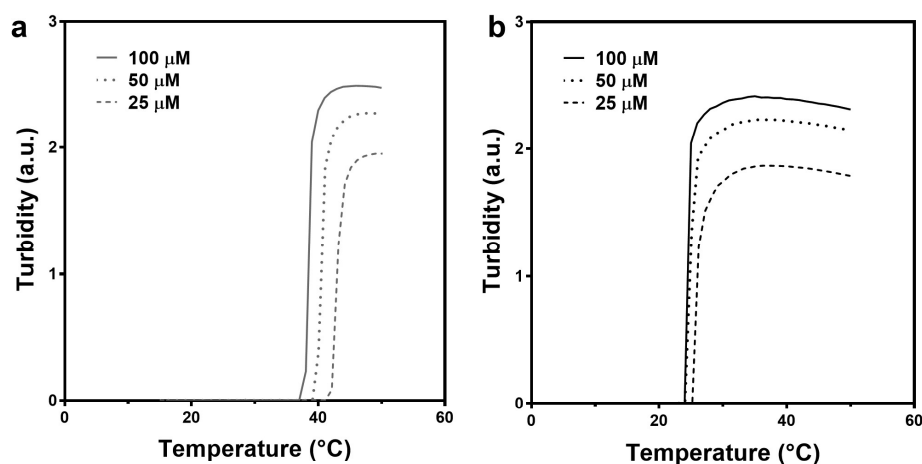
Supplementary Figure 20. a) Temperature-programmed turbidimetry assay of ELP. b) Temperature-programmed turbidimetry assay of M-ELP. See Supplementary section 7 on page 13 for the synthesis of M-ELP.
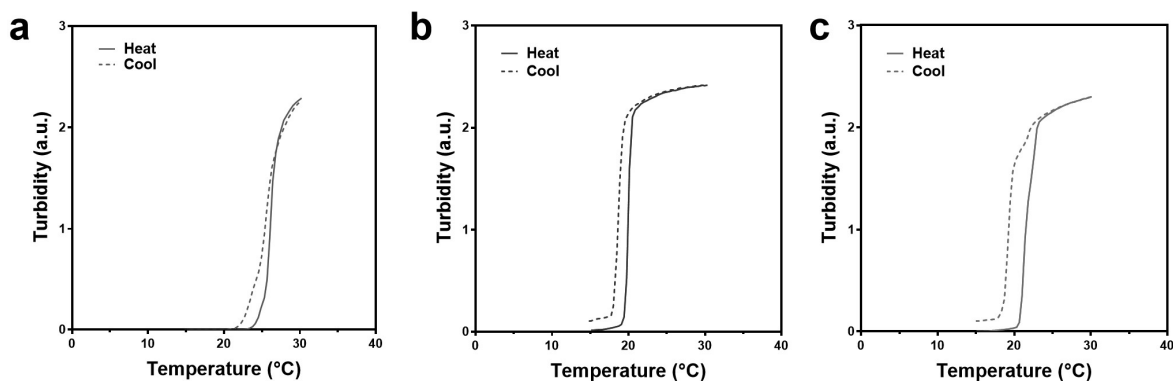
Supplementary Figure 21. Temperature-programmed turbidimetry assay demonstrates that the phase transition of FAMEs is reversible at lower temperature. a) M-B₁-ELP b) M-B₂-ELP c) M-B₃-ELP. Each construct was prepared at 100 μM.
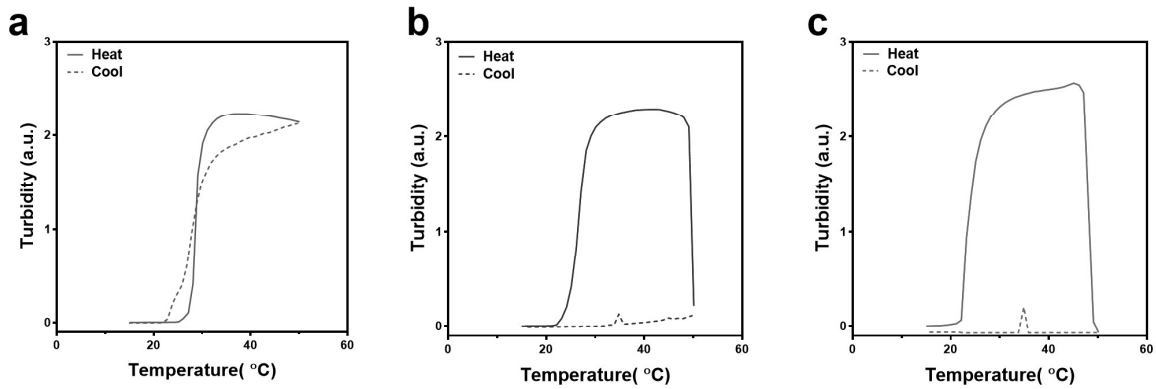
Supplementary Figure 22. Temperature-programmed turbidimetry assay demonstrates the phase-transition of M-B$_1$-ELP is reversible up to 50 °C but the phase transition of M-B$_2$-ELP and M-B$_3$-ELP is not reversible. Each construct was prepared at 50 μM.
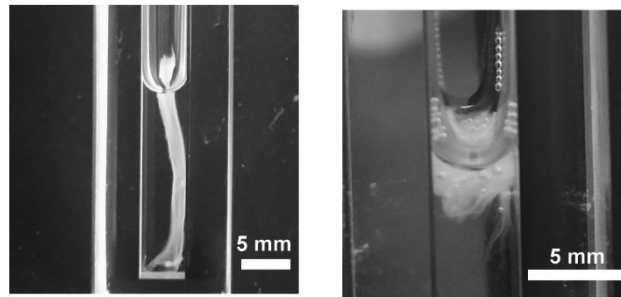
Supplementary Figure 23. Additional optical images of the structures formed by the M-B$_2$-ELP (left) and M-B$_3$-ELP constructs (right).
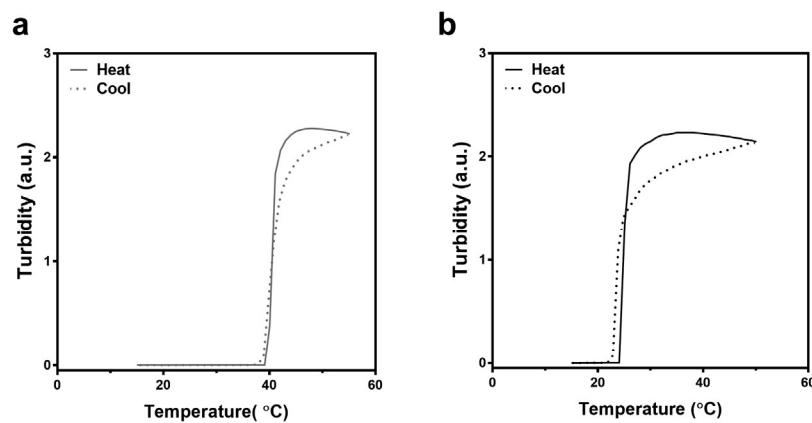
Supplementary Figure 24. Temperature-programmed turbidimetry assay demonstrates that the phase transition of ELP and M-ELP is reversible up to 50 °C. Each construct was prepared at 50 μM.
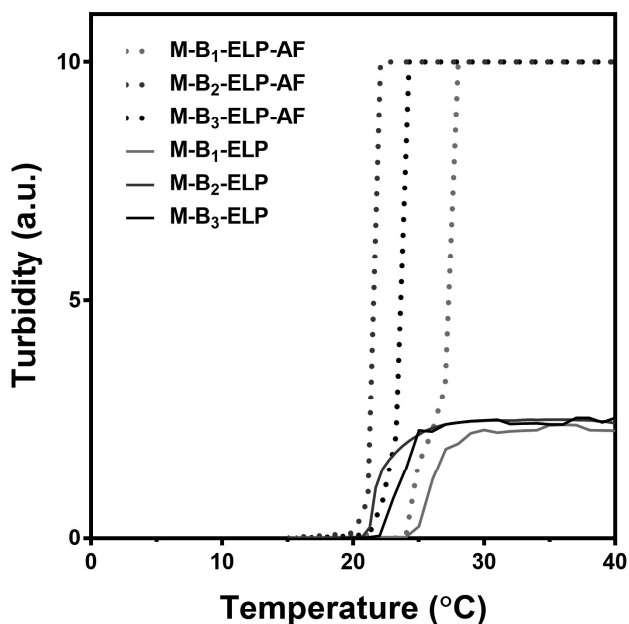
Supplementary Figure 25. Temperature-programmed turbidimetry assay demonstrates that labeling with Alexa Fluor 488 does not change the phase transition of ELPs. The higher absorbance of the labeled samples (M-B₁₋₃-ELP-AF) is due to the smaller size of the chamber window in the microcuvettes used. Each construct was prepared at 100 μM.

11. Dynamic Light Scattering

Dynamic light scattering (DLS) studies were conducted to investigate the self-assembly of various constructs in solution. Prior to analysis, samples were freshly prepared in PBS to a concentration of 50 μM and filtered through a 0.22 μm polyvinylidene fluoride membrane (Durapore) directly into the quartz cell. DLS experiments were conducted in a temperature-controlled DynaPro Microsampler (Wyatt Technologies). Measurements were obtained over a temperature range of 4 °C to 10 °C using 0.5 °C steps and 18 acquisitions of 5 s each for every temperature point. Autocorrelation intensities across the range of temperatures were averaged and plotted as a function of decay time with error bars representing the standard deviation of measurements (shown in Figure 3a as a shaded band around each line).

We note that it is not possible to extract reliable size data (R_h) from the DLS autocorrelation function of myristoylated constructs, as most DLS models are developed by assuming a spherical object as the source of scattering. The electron microscopy (Figure 4a-c) shows that all the

constructs have a structure that significantly deviates from a spherical state, thus undermining the validity of the underlying assumptions in the DLS analysis models.

12. Circular Dichroism

We probed the secondary structure of all the constructs using circular dichroism (CD) to study whether the incorporation of the short recognition sequences or myristoylation significantly altered the secondary structure of the constructs. CD spectroscopy was performed using an Aviv Model 202 instrument and a 1 mm quartz cell (Hellma). Each sample was freshly prepared by dissolving the lyophilized product in a salt-free phosphate buffer solution (pH 7.4, Sigma Aldrich) to a concentration of 10 μM. This solution was stored on ice prior to analysis. The CD spectra were obtained at 15 °C from 350 nm to 180 nm in 1 nm steps and 0.5 s averaging time. The CD spectra were corrected for the buffer signal at 15 °C. Each experiment was repeated in triplicate, and the average of the three measurements was represented as a mean residue ellipticity ($[\Theta]$, deg cm^2 dmol^{-1}). Data featuring dynode voltages above 500 V was not considered for analysis.[11] The CD data for different constructs were then normalized at 220 nm for comparison.
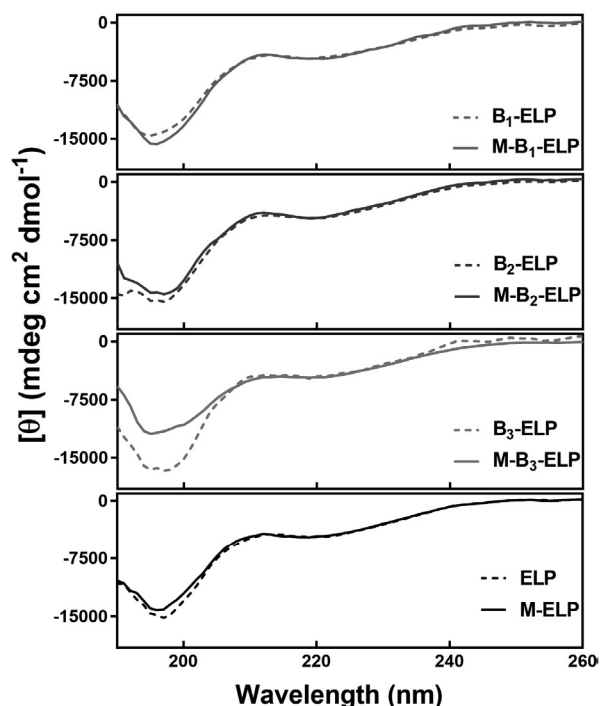
Supplementary Figure 26. Circular dichroism of FAMEs, B$_{1-3}$-ELP, M-ELP and ELP controls at T = 15 ºC < T$_t$. The secondary structure of controls and FAMEs have significant similarities, and myristoylation does not result in major changes in the secondary structure.

We investigated the effect of myristoylation on the secondary structure of the ELPs using CD. In accordance with the turbidity profile, non-myristoylated ELPs exhibited CD signatures characteristic of canonical ELPs (Supplementary Figure 26), featuring a primary negative peak at 195 nm and a secondary negative peak at 220 nm (dashed lines, Supplementary Figure 26). The primary negative peak is commonly attributed to random coils, while the secondary peak is assigned to transient β-turn and β-spiral structures, resulting from the periodic placement of Pro-Gly units along the ELP backbone.[12] Myristoylated ELPs (solid line, Supplementary Figure 26) exhibited a similar CD signature; however, the intensity of the negative peak at 195 nm was slightly reduced for M-B$_3$-ELP (solid red line, Supplementary Figure 26).

Due to the limited solubility of synthetic PAs in water and PBS, it was not possible to compare their CD spectra with ELPs as a control. However, based on previous reports of PAs, it is likely that the first 4-6 amino acids in the recognition sequence adopts a β-sheet conformation after the conjugation of the myristoyl group, characterized by two peaks at 195 nm and 220 nm.[13] The positive peak at 195 nm, indicative of β-sheet structures, overlaps with the much stronger negative peak from the ELPs. Due to similarities between the CD signature of ELPs and FAMEs, we can conclude that myristoylation did not significantly increase the beta-turn population, nor did it result in a global change in the conformational preference of the ELPs. We also point out that the CD signature of FAMEs (particularly M-B$_3$-ELP) may be less reliable due to the self-assembly and aggregation of these constructs in solution.[14]

13. FT-IR

We collected Fourier transform infrared spectroscopy (FT-IR) spectra on a Nicolet 8700 FT-IR spectrometer that was equipped with an attenuated total reflectance attachment. A Ge crystal was used for collecting spectra of the proteins and peptides. In bench mode operation, the lyophilized powder was clamped tightly over the Ge crystal, and the spectra were collected from 4000 to 400 cm^{-1} with 1 cm^{-1} resolution. There were 128 scans accumulated per spectrum.

We utilized FT-IR spectroscopy to probe the effects of myristoylation on the conformation and hydrogen bonding of the amide carbonyls (Figure 3b). Consistent with our interpretation of the CD spectra, both non-myristoylated and myristoylated ELPs exhibited similar FT-IR spectra. In both cases, the amide I bond displayed a characteristic low-frequency component around 1615 cm^{-1} and a high frequency component near 1650 cm^{-1}, consistent with previous reports for ELPs.[15]

However, the control PA spectra exhibited a much more complex absorption pattern consistent with the presence of β-sheet structures in the lyophilized powder while demonstrating that the internal dynamics of each PA is dictated by the sequences preceding the hydrophobic tail (Supplementary Figure 27).[4,16]
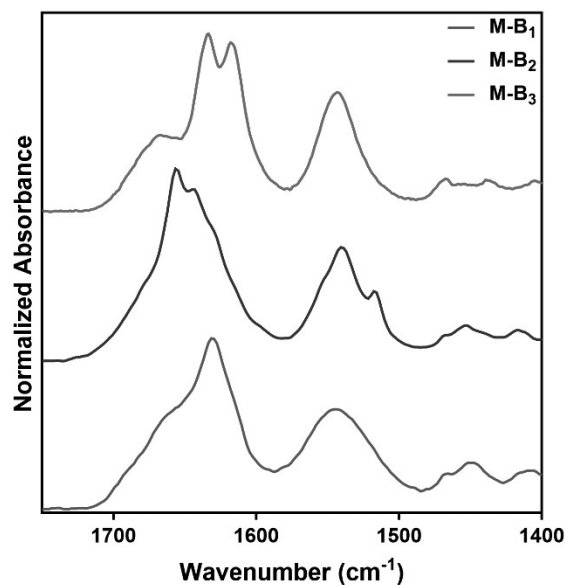
Supplementary Figure 27. Stacked FT-IR spectra of M-B₁ (green), M-B₂ (blue), and M-B₃ (red) demonstrates the different internal dynamics of these PAs.

14. Variable Temperature ATR-IR

<u>Sample Preparation</u>

Variable temperature ATR-IR experiments were performed in Max Planck Institute for Polymer Research (Mainz, Germany). Each sample was prepared to the final concentration of 100 μM solution by dissolving lyophilized powder in cold (~ 4 °C) Dulbecco's Phosphate Buffered Saline (PBS, Thermo Fisher Scientific). After the addition of cold PBS, the solution was immediately mixed by vortex and left in a thermomixer (Eppendorf) at 4 °C while shaking for 30 min. From this point onward, the prepared solutions were kept in an ice bath between the ATR-IR measurements.

<u>Variable temperature ATR-IR experiment</u>

ATR-IR measurements samples were performed with FT-IR Bruker TENSOR II spectroscopy (Bruker, Germany) with a diamond crystal. The samples were loaded into a metallic sample holder with an inner volume of ~ 0.5 mL, which was pressed on the top of the ATR crystal. A refrigerated / heated circulator (Julabo, Seelbach, Germany) combined with a custom-built copper tube was used to heat or cool the metallic sample holder by fitting the copper tube around the metallic holder. As the solution was in contact with the metallic holder, this device cooled or heated the sample solution on the ATR crystal. The metallic holder design allowed us to measure the temperature of the solution during measurement with a thermocouple and digital multimeter (Voltcraft VC 140). Before each ATR measurement of protein samples, a solution of PBS was used to verify the temperature settings on the circulator. After verification, the proper temperature was set in the circulator, the neat PBS was taken out from the sample holder, and the container was filled with the measured sample –while still monitoring the temperature. ATR-IR spectra were collected at 10°C, 30°C, and 50°C from 400–4000 cm^{-1} with an accumulation of 128 scans and using a spectral resolution of 4 cm^{-1}.

Data processing

At least three different ATR-IR spectra from each sample were collected at each temperature. Data analysis of the ATR-IR spectra was done by using IgorPro (Wavemetrics, Lake Oswego, OR). First, the baseline of spectra was corrected by subtracting the average absorbance value which was calculated from the absorbance values between 3877 cm^{-1} and 3997 cm^{-1} from each ATR-IR spectrum. All spectra of each sample at a certain temperature were averaged and the ATR-IR spectra of PBS at the same temperature was subtracted to produce difference spectra.

Supplementary Table 6. ATR-IR peak assignment and references

peak assignment	wavenumber	reference
CH_3 asymmetric	1450 ± 20 cm^{-1}	15,17,18
Amide II band	1500 cm^{-1} – 1600 cm^{-1} (Max absorbance at 1540 cm^{-1})	17
β-spiral signature in Amide I band	1615 cm^{-1} and 1656 cm^{-1}	15

Little, if any, signal was seen at 10 °C for any of the proteins at this concentration. Notably, M-ELP showed an almost identical spectrum at 30 °C and 50 °C (Figure 3c). However, the raw signal intensity for M-ELP was lower than $M-B_1-ELP$ at 50 °C (data not shown). This suggests that M-ELP coacervates are not significantly dehydrated at higher temperatures. This observation is

consistent with the relative constant size of coacervates observed in the wide-field microscopy at 30°C and 50°C (Supplementary Figure 32b, c).
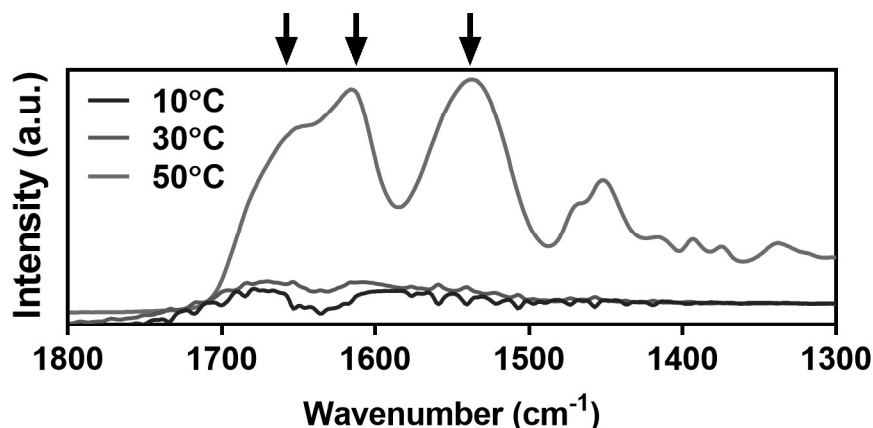
Supplementary Figure 28. Variable temperature ATR-IR experiment for ELP control at 10, 30 and 50 °C (red, green, and blue lines respectively). The arrows denote the location of two components of amide band I and amide band II.

15. Thioflavin T (ThT) assay

15.1 Single Time-Point Static ThT Assay

The static ThT assay was conducted on a SpectraMax M series microplate reader. ThT stock solution (50x) was freshly prepared by dissolving 8 mg of ThT in 10 mL of PBS, which was then kept in the dark. This solution was furthered diluted by a factor of 5 to obtain the working stock solution (10x). A freshly prepared sample of each construct (144 µL) was mixed with the ThT (16 µL). Each sample contained 100 µM of protein in addition to 50 µM of ThT and was kept on ice prior to the experiment. The mixture (130 µL) was then transferred to a black Corning® 96 well half area plate with a clear flat bottom and was incubated for 5 minutes at 20 °C. The ThT fluoresce (excitation wavelength = 440 nm, emission wavelength =482 nm) for each sample was recorded.

15.2 Dynamic ThT Assay

We conducted a ThT assay on a StepOnePlus Real-Time PCR System by adapting a procedure commonly used for protein thermal shift assays. ThT stock solution (50x) was freshly prepared by dissolving 8 mg of ThT in 10 mL of PBS, which was then kept in the dark. This solution was furthered diluted by a factor of 5 to obtain the working stock solution (10x). A freshly prepared sample of each construct (18 µL) was mixed with the ThT (2 µL). Each sample contained 100 µM of protein in addition to 50 µM of ThT and was kept on ice prior to the experiment. We used the

FAM™ filter in the instrument for measuring the ThT signal. Control experiments without protein and/or ThT were conducted in tandem to ensure that the fluorescent signal was due to the interaction of the proteins with the ThT. Samples were incubated at 4 °C for 10 min before the start of the experiment. Fluorescence was measured as the temperature was increased to 60 °C at a rate of 1% according to the instrument setting (i.e., approximately 1 °C/min). A baseline correction was conducted using the TN020 procedure package in Igor Pro 6.37 software.

We suggest that the differences in ThT fluorescence between M-ELP and ELP in static assay can be explained by considering the peptide sequences after myristoyl group. The M-ELP sequence consists of Myristoyl-GVGVP and valine residues have a relatively high β-sheet propensity (Supplementary Table 1). It is likely that this short peptide sequence adopts an amyloid cross-section and thus interact strongly with the ThT dye at low temperature.

However, presence of proline as the fifth residue in the M-ELP sequence (Myr-GVGVP) is likely to break the formation of secondary content after this position. Thus, despite having two residues with high β-sheet propensity, an extended β-sheet cannot be formed with this sequence. This hypothesis can explain the lower interaction of M-ELP with ThT at higher temperature.

We are also mindful that ThT fluorescence depends on parameters such as the solvent viscosity (which is expected to change at least in the ELP coacervates).[19,20] Considering these factors, we suggest that the interaction of FAMEs with ThT can be enhanced through any of the following pathways at higher temperatures. 1) It is possible that a segment of the ELP domain, close to the PA-domain, is restricted to a conformation with favorable interactions with the ThT dye. Our variable temperature ATR-IR experiments (Figure 3c) provides a support for this hypothesis as the broad amide peaks in the ELP and M-ELP are replaced with more well-defined sharper peaks. 2) Above T_t, the core of the FAME aggregates (PA-domain) can grow as the aggregates are no longer stabilized by the dehydrated ELP corona. This extended core can interact with more ThT molecules. In particular, this pathway is consistent with microscopy results obtained for M-B_2-ELP (Figure 4h,k). 3) The increased viscosity of the ELP coacervates can also increase the ThT fluorescence above T_t.

Our current mechanism does not explain the small decrease in ThT fluorescent signals for ELP and M-ELP at high temperatures (with an inflection point ~ 50 °C. We are tempted to assign this observation to settling of some of the ELP coacervates to the bottom of the tube at high temperatures which remove some of the entrapped ThT molecules. It is shown by others that

presence of charged amino acid (in this case, Arg which is found in all recognition sequences but not in ELP or M-ELP) can also affect the kinetics of coacervate coalescence.[21]

16. Spinning Disk Confocal Laser Microscopy (SDCLM)

SDCLM was conducted on an Olympus SD-OSR System based on IX83 inverted microscope equipped with Yokogowa W1 Spinning disk confocal with 50 nm disk and Tokai Hit WSKM environmental control module. The spatial distribution of the fluorophore-labeled FAMEs was characterized via fluorescence microscopy using a 100X Si oil objective with correction collar and the appropriate filter set (excitation BP 470/40, emission BP 525/50). Fluorescence intensities of the acquired images were analyzed using Metamorph acquisition software.

SDCLM enjoys the sensitivity and the resolution of traditional confocal microscopy but offers the advantage of faster data acquisition over a larger area of the sample. We leveraged these capabilities to visualize the fine details self-assembly process. SDCLM was conducted by depositing 20 µL of the fluorescently labelled protein samples below T_t onto a glass bottom MatTek dish (Ashland, MA) and transferring the slide to microscope stage and heating it to 30 °C. We monitored the assembly by taking consecutive images from a focal plane above the cover slips to avoid surface induced artifacts. The temperature was then raised to 50 °C to monitor the final stage of the self-assembly. Following the stabilization of the network, we also used the super resolution mode[22] of the microscope and recorded multiple images at different focal planes and collapsed these z-stack images using ImageJ to visualize finer details of the final entangled network.

17. Encapsulation and Imaging

We also visualized the phase transition of FAMEs and ELPs in monodisperse, well-defined droplets at micron-level resolution during the second and third stages of self-assembly. We chose this system because it prevents the coalescence of aggregates beyond the well-defined boundaries of each micron-scale droplet, which is ideal for studying the morphogenesis of structures at the micro-scale.[23] To visualize the self-assembled structures, we genetically encoded a Lys residue at the C-terminus of the M-B$_{1-3}$-ELP constructs to enable labeling with Alexa Fluor® 488 dye. The turbidity profile of these labeled FAMEs was identical to their parent sequences (Supplementary Figure 25), indicating that the addition of a Lys and a fluorophore at a position distant from the PA domain does not perturb the self-assembly process. We then used a microfluidic device to form

water-in-oil emulsions containing each FAME at 100 μM. The structural evolution of each construct was then visualized using wide-field fluorescence microscopy while increasing the temperature from 10 °C to 50 °C at a rate of 1 °C/min.

17.1 Droplet Formation

The droplets were prepared by following an established method previously reported elsewhere.[23] Microfluidic water-in-oil droplet generators were purchased from Dolomite Microfluidics. To create aqueous droplets, we injected two liquid phases – a dispersed aqueous phase of the FAME sample, and an organic continuous phase comprised of TEGOSOFT® DEC/ABIL® EM 90/mineral oil (75/5/20 v/v%) – into the drop generators at constant flow rates using precision syringe pumps. We tuned the flow rates of the dispersed and continuous fluids to ensure droplet formation in the dripping regime and used a constant flow rate of 250 $\mu L.hr^{-1}$ for the organic continuous phase and 75–100 $\mu L.hr^{-1}$ for the aqueous, dispersed phase. We monitored the production of droplets within the microfluidic device using a 5× objective on an inverted microscope (Leica) equipped with a digital microscopy camera (Lumenera Infinity 3-1 CCD).

The organic phase contains commercially available surfactants to stabilize aqueous droplets. In our previous work (reference 22) and current work, we have noticed that this mixture does not affect the cloud point (T_t) of ELPs. However, we have performed the following control experiment to ensure that the surfactants do not perturb the self-assembly of FAMEs. We have mixed PBS (1 mL) with the organic phase (containing the same three components described above) by vigorous agitation on a vortex. After waiting for 1 hour, the cloudy mixture separated into three layers, oil phase at top, narrow emulsion layer at the middle, and a PBS phase at the bottom. We carefully removed the top layer and dissolved the M-B_2-ELP in this mixture to the final concentration of 50 μM. As a control, M-B_2-ELP was dissolved in PBS to the similar concentration. The phase behavior and self-assembly of both samples were analyzed by a turbidimetry assay as described in Section 10. Both samples exhibited almost identical T_t, T_c (the onset of reduction of turbidity, Supplementary Figure 29a), and overall macroscopic morphology (Supplementary Figure 29b).
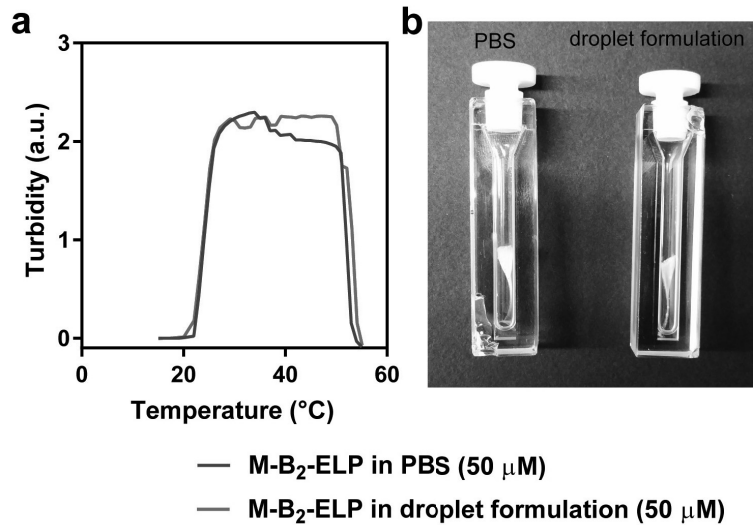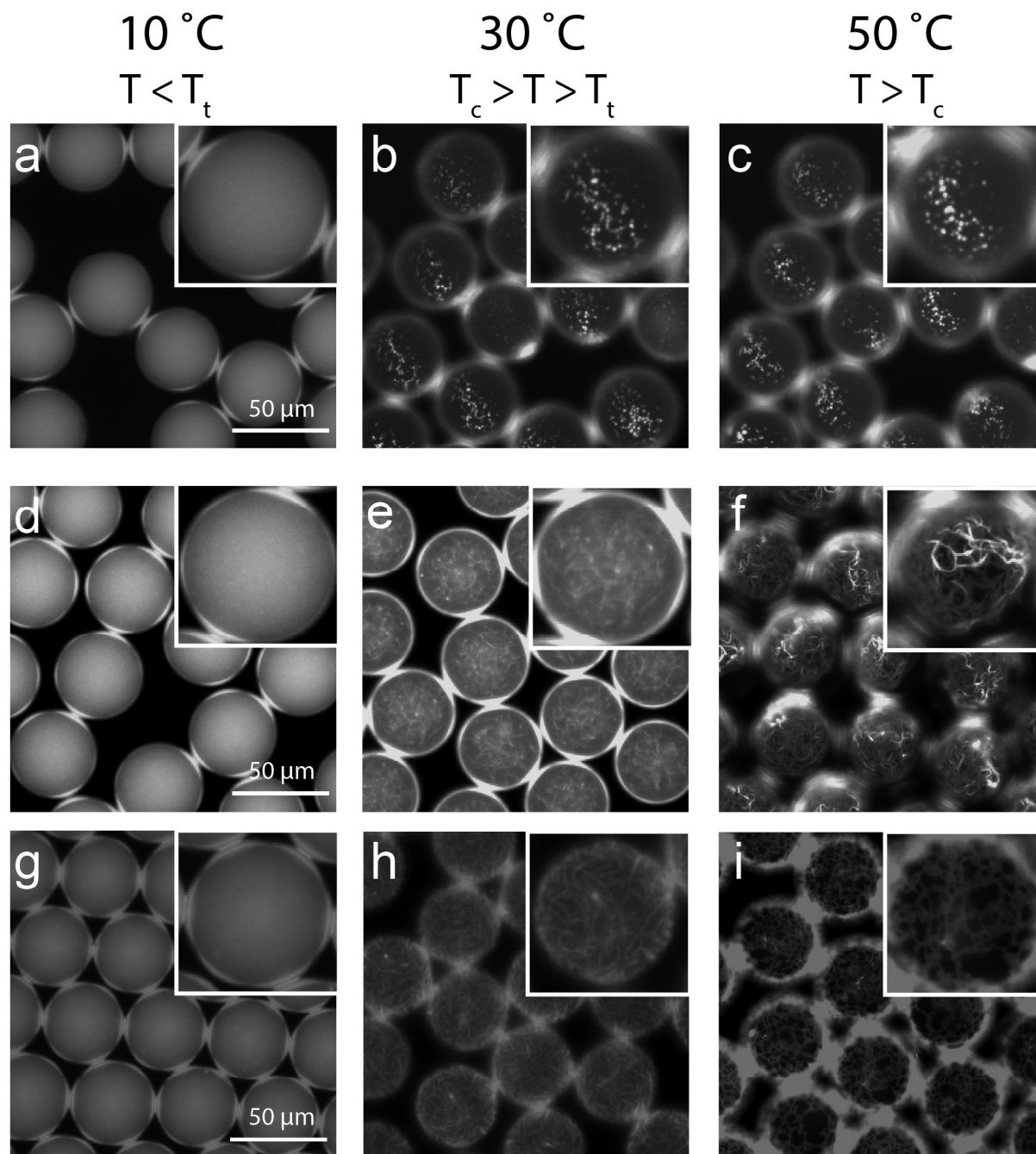
Supplementary Figure 29. Temperature-programmed turbidimetry assay demonstrates that the (a) phase transition and (b) self-assembly of FAMEs are not affect by the surfactants in the droplet system.

Additionally, the bundles of fibers observed in Supplementary Figure 30f is reminiscent of morphology observed by SEM (Figure 5a). We also point out that the we have conducted the confocal microscopy in the absence of droplet encapsulation and the results of these experiments are also in good agreement with droplet system. Nonetheless, we are still mindful that the self-assembly of the amphiphilic FAMEs can be affected by the presence of surfactants near the droplet interfaces.

17.2 Visualization of the FAME Constructs' Thermally Triggered Phase-Transition

The FAME emulsion samples were collected on a glass microscope slide and heated using a precision Peltier heating and cooling stage (Linkam LTS120) equipped with a Linkam PE95 digital temperature control unit. The spatial distribution of the fluorophore-labeled FAMEs was characterized via fluorescence microscopy using an upright Zeiss Axio Imager A2 microscope with a 20× objective and the appropriate filter set (excitation BP 470/40, emission BP 525/50). Fluorescence intensities of the acquired images were analyzed using Zeiss ZEN imaging software. M-B$_2$-ELP and M-B$_3$-ELP fluorophores were artificially colored blue and red in the images in Supplementary Figure 30 for distinction and clarity.

Supplementary Figure 30. Visualization of the temperature-triggered phase transition and self-assembly of FAMEs using fluorescence microscopy at stages 2 and 3: (a-c) M-B₁-ELP transitions into liquid-like coacervates similar to canonical ELPs. (d-f) M-B₂-ELP transitions into short, disordered fiber-like structures before transitioning into a highly-packed network of fibers at higher temperatures. (g-i) M-B₃-ELP transitions into a network of interconnected fibers. Images in (a-i) were obtained from FAMEs encapsulated in water-in-oil emulsified droplets. Fluorophores were artificially colored blue for M-B₂-ELP (d-f) and red for M-B₃-ELP (g-i) in these images for distinction and clarity.

At 10 °C (T < T_t), a homogeneous fluorescent signal was detected across each droplet (Supplementary Figure 30a, d, and g), suggesting that at stage 1 (T < T_t) each population of the FAMEs exists as a nanoscale assembly below the diffraction limit, which is consistent with DLS (Figure 3a). However, the N-terminal PA-domain significantly altered the morphogenesis of aggregates at higher temperatures. During stage 2, at 30 °C (T_c > T > T_t), M-B_1-ELP, whose PA domain has the lowest propensity to form β-sheets, formed spherical liquid coacervates (Supplementary Figure 30b) that resemble canonical ELPs[23] (Supplementary Figure 31). These liquid coacervates remained stable at 50 °C (T > T_c, Supplementary Figure 30c) and were reversibly dissolved as the temperature was lowered back below T_t, further demonstrating their similarity to canonical ELPs. At 30 °C (T_c > T > T_t), M-B_2-ELP transitioned into an entangled network of small fibers (Supplementary Figure 30e), with no apparent long-range order. However, as the temperature was increased to 50 °C (T > T_c), these shorter fibers coalesced to form longer fibers that stacked together and exhibited order at the microscale (Supplementary Figure 30f). In contrast, M-B_3-ELP, which has the highest propensity to form β-sheets, assembled into an entangled network of long fibers (Supplementary Figure 30h) at 30 °C. The resulting network underwent compaction at 50 °C, but we did not observe fiber stacking and microscale assembly (Supplementary Figure 30i). We are mindful that slight differences in the heating profile used in wide-field fluorescence microscopy and SDCLM may impact the final structure of the aggregates, but these two experiments corroborate each other and provide an informative first-hand view of the self-assembly progression.
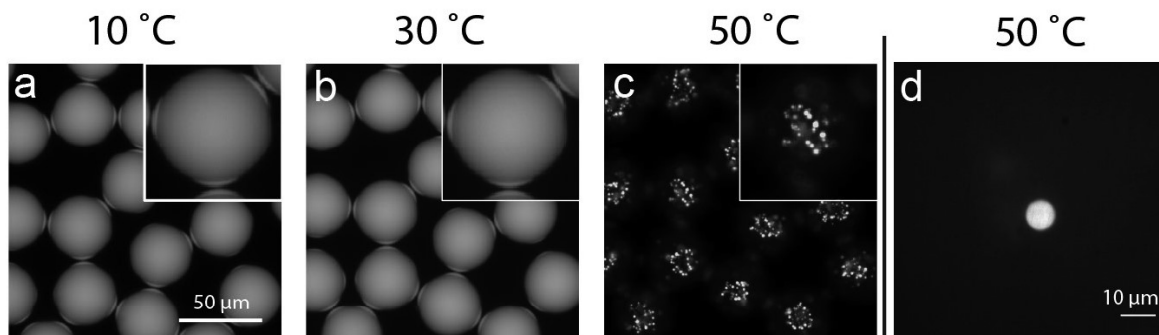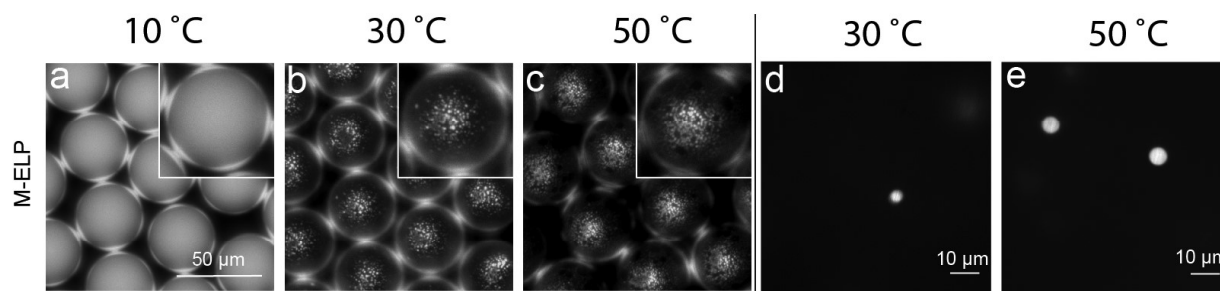

Supplementary Figure 31. Visualization of temperature-triggered phase transition and self-assembly of canonical ELP using fluorescence microscopy. (a-c) Control ELP transitions into liquid-like coacervates at temperatures above its T_t (~ 40 °C at 100 μM). (d) Confocal microscopy images of a coacervate at 50 °C. Images in (a-c) were obtained from ELP encapsulated in water-in-oil emulsified droplets.

Supplementary Figure 32. Visualization of temperature-triggered phase transition and self-assembly of M-ELP using fluorescence microscopy. (a-c) M-ELP transitions into liquid-like coacervates at temperatures above its T_t (~ 25 °C at 100 µM). Confocal microscopy images of coacervates at 30 °C (d) and 50 °C (e). Images in (a-c) were obtained from M-ELP encapsulated in water-in-oil emulsified droplets.

18. Cryo- Transmission Electron Microscopy (TEM)

Cryo-TEM experiments were performed at Duke University Shared Materials Instrumentation Facility. Lacey holey carbon grids (Ted Pella, Redding, CA) were glow discharged in a PELCO EasiGlow Cleaning System (Ted Pella, Redding, CA). A 3 µL drop of the sample (100 µM of each construct) at 20 °C ($T < T_t$) and 30 °C ($T_c > T > T_t$) was deposited onto the grid, blotted for 3 s with an offset of −3 mm, and vitrified in liquid ethane using the Vitrobot Mark III (FEI, Eindhoven, Netherlands). The sample chamber was maintained at 100% relative humidity to prevent sample evaporation. Grids were transferred to a Gatan 626 cryoholder (Gatan, Pleasanton, CA) and imaged with an FEI Tecnai G^2 Twin TEM (FEI, Eindhoven, Netherlands), which was operated at 80 keV.[24] Control PAs (M-B$_{1-3}$) were resuspended in 20% aqueous acetic acid solution (v/v%) due to their low solubility in PBS or water. Cryo-TEM confirmed that control PAs (M-B$_{1-3}$) at 20 °C primarily formed fibers and sheets with large aspect ratios, featuring diameters equal to 11.8 ± 2.9 nm, 9.7 ± 2.7 nm, and 13.9 ± 0.9 nm (mean ± s.e.m.), respectively (Supplementary Figure 33a-c), consistent with the behavior of previously reported canonical PAs.
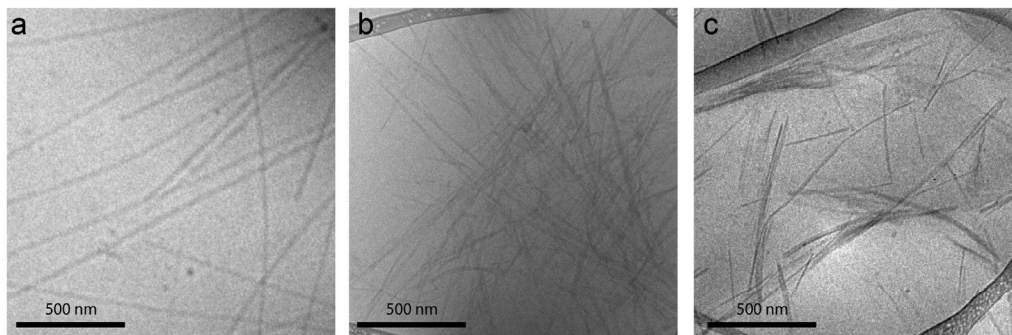
Supplementary Figure 33. Cryo-TEM of control PAs at 20 °C, a) M-B$_1$, b) M-B$_2$, and c) M-B$_3$ demonstrates that they form fibers and sheets commonly observed with canonical PAs. All PAs were dissolved in 20% aqueous acetic acid due to their low solubility in PBS
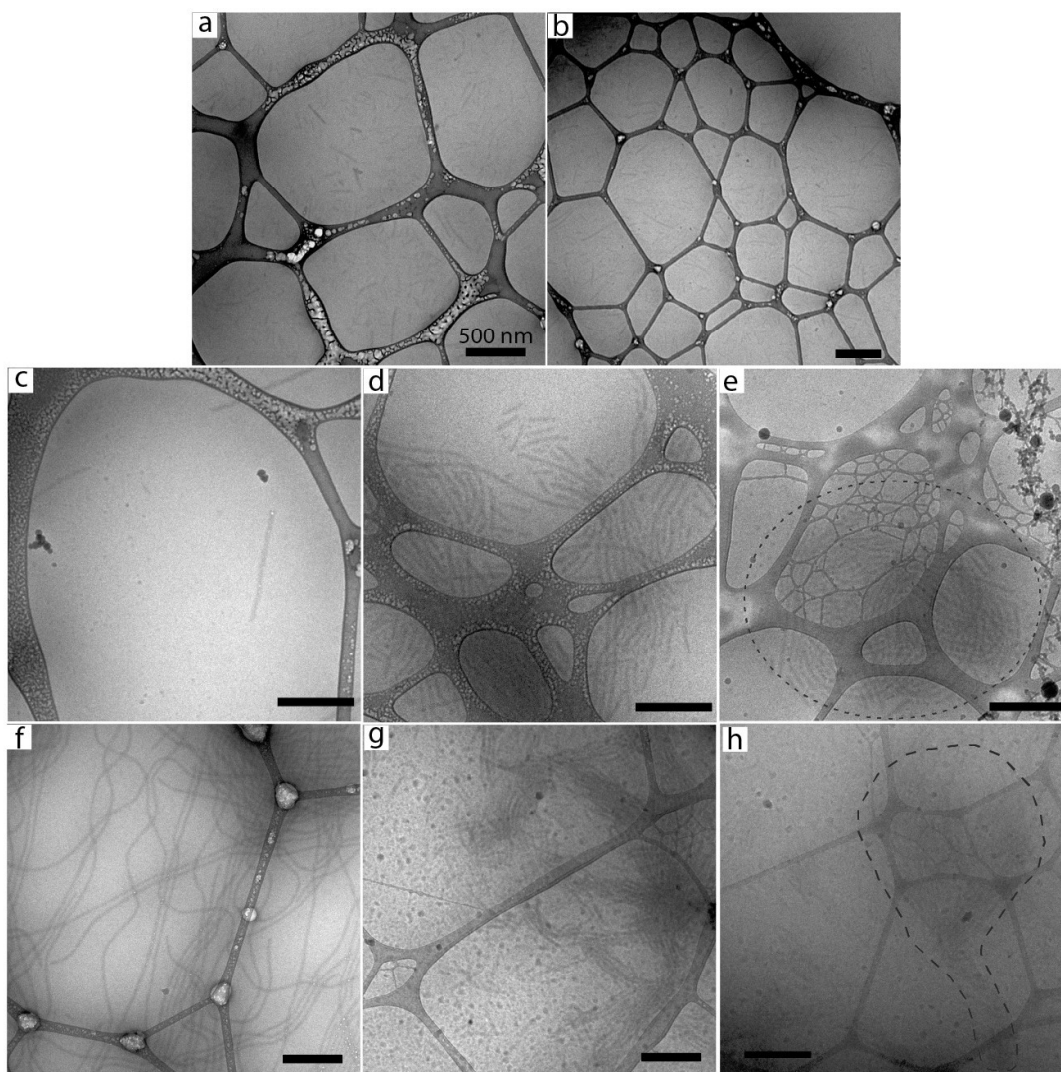
Supplementary Figure 34. Additional cryo-TEM images of the self-assembled M-B$_1$-ELP at 20 °C (a, b), M-B$_2$-ELP at 20 °C (c), and 30 °C (d, e). The blue dashed line is added to panel

(e) to highlight the boundary of coacervate cross-section. Additional cryo-TEM images of the self-assembled M-B$_3$-ELP at 20 °C (f) and 30 °C (g, h). The blue dashed line is added to panel (h) to highlight the boundary of coacervate cross-section.

19. Scanning Force Microscopy

Scanning Force Microscopy was performed at the Physics at Interface Group at the Max Planck Institute for Polymer Research in Mainz, Germany. We prepared a 100 μM solution of FAMEs in cold PBS buffer. Then 1.5 μl of the solution was put in an Eppendorf tube and heated to 30 °C for typically 1 - 2 min in a water bath. Then the entire solution was pipetted onto a freshly cleaved mica substrate and then carefully dried in an air stream. Subsequently the surface was rinsed with pure water provided by a Sartorius Arium 611 VF purification system (Milli-Q, specific resistivity of 18.2 MΩ·cm). Then the sample was dried again in an air stream and installed on the xy-stage of a Dimension ICON SFM instrument (Bruker, Karlsruhe, Germany). For the SFM investigation we used Olympus AC240TS cantilevers having a nominal spring constant of 2 N/m. The SFM was operated in the peak force tapping mode at 1 kHz. For all studies, we simultaneously recorded the surface topography, the adhesion, and the DMT modulus maps (based on the model of Derjaguin-Muller-Toporov).[25]

It is important to note that the presence of a surface during preparation my lead to changes in the aggregation behavior. In particular, we propose that M-B$_1$-ELP with the lowest β-sheet propensity is more prone to exhibit such behavior as PA-domain core is held together by weaker attractive forces (Supplementary Figure 35b) and the structure can be affected through interaction with mica surface. This hypothesis can explain the observed sub-population of spherical aggregates for M-B$_2$-ELP (Supplementary Figure 35c-d).
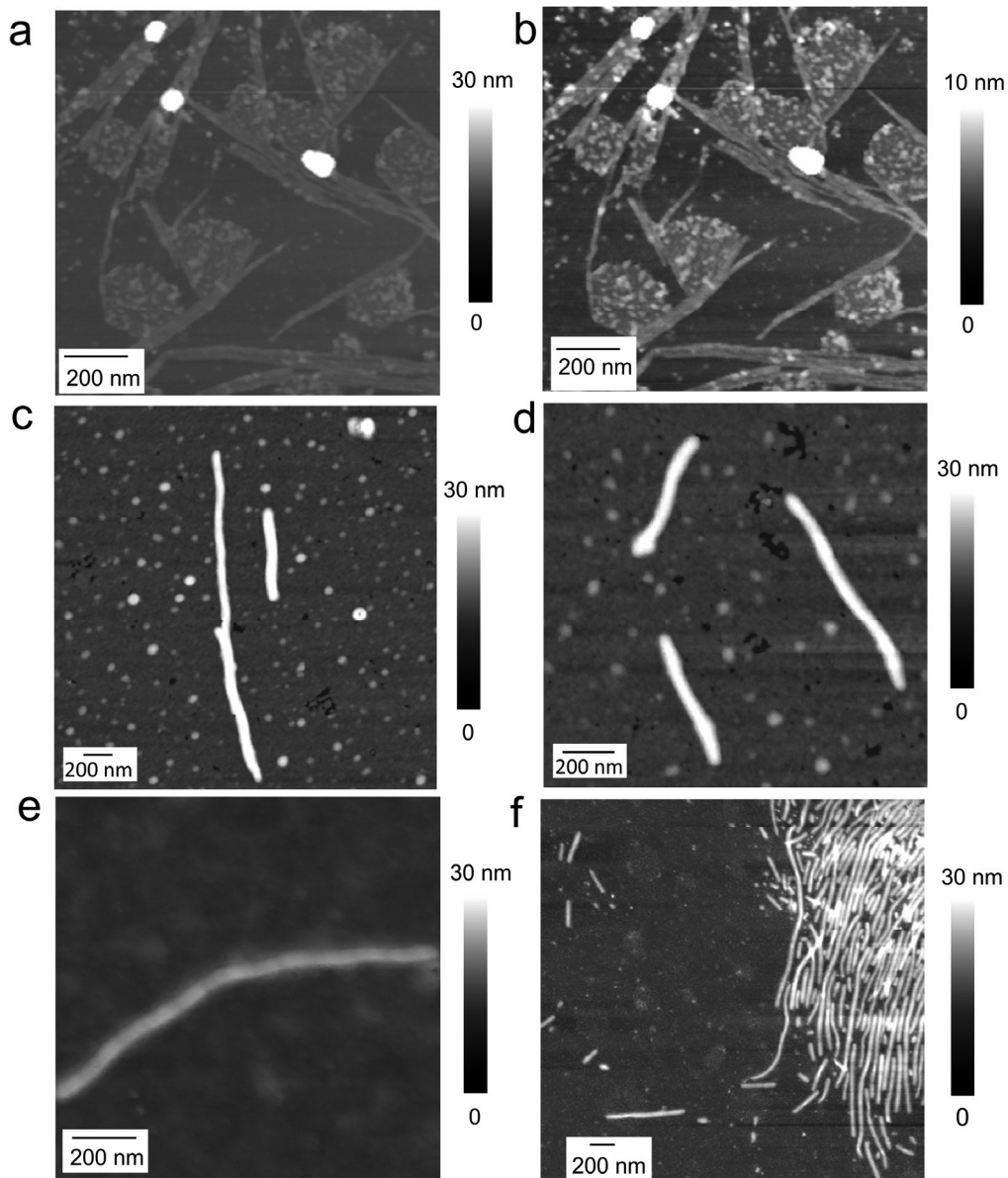
Supplementary Figure 35. Additional SFM images of M-B₁-ELP (a, b). The topographic image is provided with a different height scale in (b) to emphasize the surface-induced aggregates that were only observed in M-B₁-ELP. Additional SFM images of M-B₂-ELP (c, d) and M-B₃-ELP (e, f).
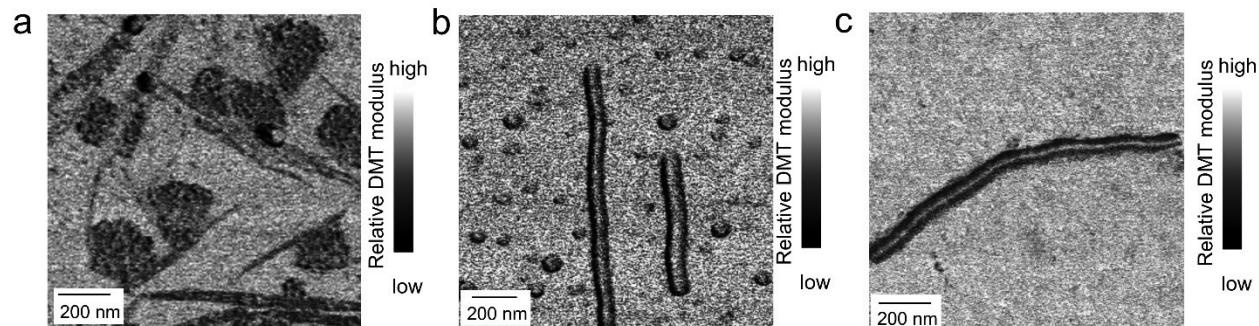
Supplementary Figure 36. The peak force mode allows to record mechanical properties of the surface such as the DMT modulus which is based on a model developed by Derjaguin-Muller-Toporov.[25] We have only provided the relative DMT modulus values as in our measurements the exact tip radius is not known. These maps were recorded simultaneously to the surface shown in Figure 35a, S35c and S35e, respectively. a) M-B$_1$-ELP, b) M-B$_2$-ELP, c) M-B$_3$-ELP. For M-B$_2$-ELP and M-B$_3$-ELP a stiffer contact mechanics was measured in the center of the fibers.

20. Cryo- Scanning Electron Microscopy (SEM)

Cryo-SEM was conducted in the North Carolina State University analytical instrumentation facility. Cryo-SEM analyses were conducted using a JEOL JSM-7600 FE SEM (JEOL USA, Peabody, MA) outfitted with an Alto-2500 preparation chamber Gatan, Warrendale, PA). The macroscopic object formed by M-B$_2$-ELP (i.e. Figure 2f) was carefully placed on the SEM stage using a tweezer and was plunge frozen in liquid nitrogen slush, then transferred under vacuum to the preparation chamber and cryo-fractured. The fractured sample was etched for 5 min at -95 °C and 4 x 10^{-6} mbar to reveal the underlying microstructure. Subsequently, the samples were allowed to cool down to -120 °C. An in situ cold magnetron coater was used to make a 5 nm thick Au/Pd coating on the etched samples. The SEM images were then taken using 15 keV accelerating voltage energy and a working distance of 5 mm under cryo-temperature. The observed microstructure (Supplementary Figure 37) is consistent with the morphology observed by SEM following fixation and dehydration. M-B$_3$-ELP structure did not survive the direct freezing and cryo-fracturing and were instead analyzed by regular SEM as described below.
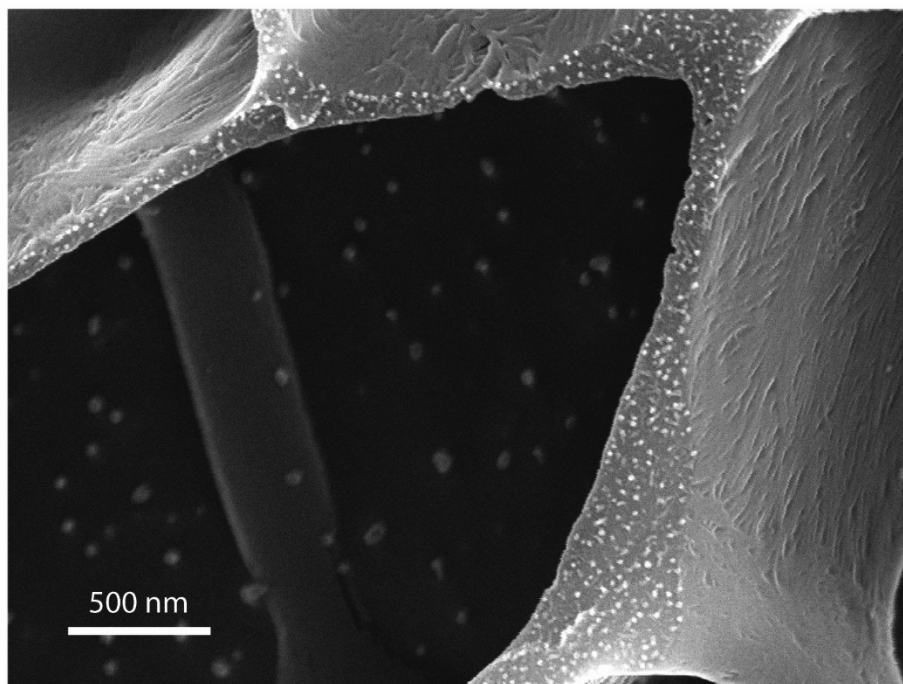
Supplementary Figure 37. Cryo-SEM of macroaggregates of M-B₂-ELP exhibits bundles of fiber similar to morphology observed by regular SEM after fixation and dehydration (see below).

21. SEM

SEM was performed at the Duke University Shared Material Instrumentation Facility using a FEI XL30 SEM-FEG instrument with an accelerating voltage of 5 kv. We used the FAMEs with a genetically encoded lysine at the C-terminal to include a chemical handle for fixation with gluteraldehyde. The assembly of M-B₂-ELP-GKG and M-B₃-ELP-GKG was triggered by heating the 750 μL of the solution of each one of the protein at the concentration of 100 μM in a UV cuvette. The solution temperature was increased at the rate of 1 °C/min from 15°C to 50 °C while monitoring the turbidity of the solution by measuring the absorbance at 350 nm. Once the temperature reached 50 °C, which coincided with the sudden decrease in turbidity, the cuvettes were removed from the instrument and the solution and the white solid structure was transferred by inversion to a 20-mL scintillation vial containing 750 μL of 8% glutaraldehyde aqueous solution (Electron Microscopy Sciences, Hatfield, PA) to achieve final glutaraldehyde concentration of 4%). After fixing the structures at room temperature for 4 hours, the structures were washed 2x with PBS before being dehydrated using increasing concentration of ethanol (30, 50, 70, 90, and 100). We prepared two replicas of each sample and dried them either using a critical

point drier (CPD, Ladd Research Industries, Williston, VT) or washed twice with hexamethyldisilazane (HMDS, Electron Microscopy Sciences). The method of drying did not seem to affect the overall morphology of the fibers for M-B$_2$-ELP-GKG. M-B$_3$-ELP-GKG did not survive CPD treatment and the SEM images were taken from the HDMS dried sample. Each sample was then fixed on the SEM stage with carbon tape and sputter coated with gold before imagining.
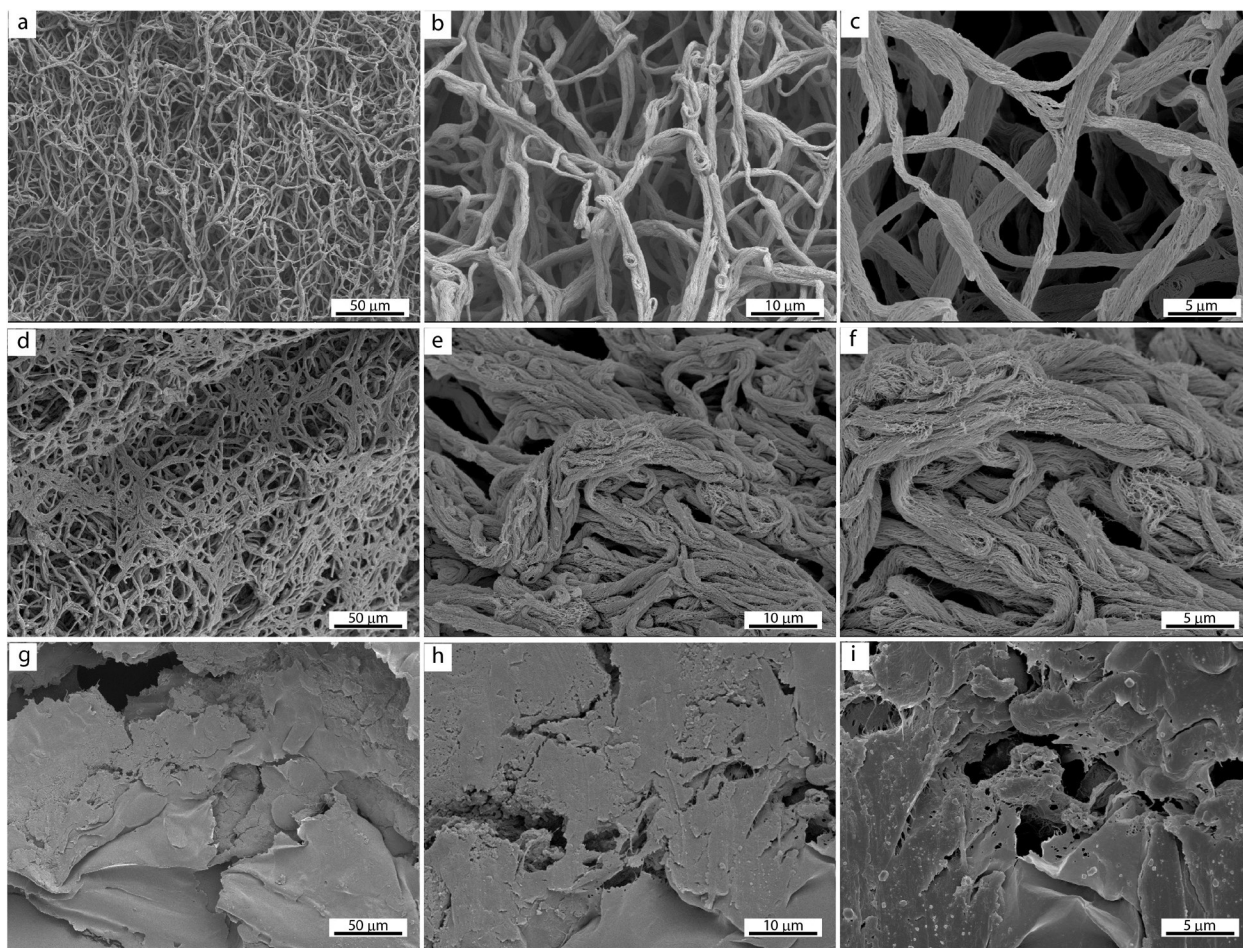
Supplementary Figure 38. Additional SEM images for M-B2-ELP at increasing magnification dried using HDMS (a-c). Additional SEM images for M-B$_2$-ELP dried using CPD (d-f). Additional SEM images for M-B$_3$-ELP dried using HDMS (g-l).

We have also used SEM to investigate the morphology of lyophilized powder of FAMEs following HPLC purification and before reconstitution in PBS (Supplementary Figure 39). Following lyophilization, we crushed a small amount of lyophilized powder to reveal internal structure and placed a small amount of lyophilized powder on the SEM stage. As explained above in section 5, HPLC purification appears to reset the self-assembly memory of the system after two rounds of ITC used for purification of proteins (i.e. no fiber is observed in the lyophilized powder after HPLC).
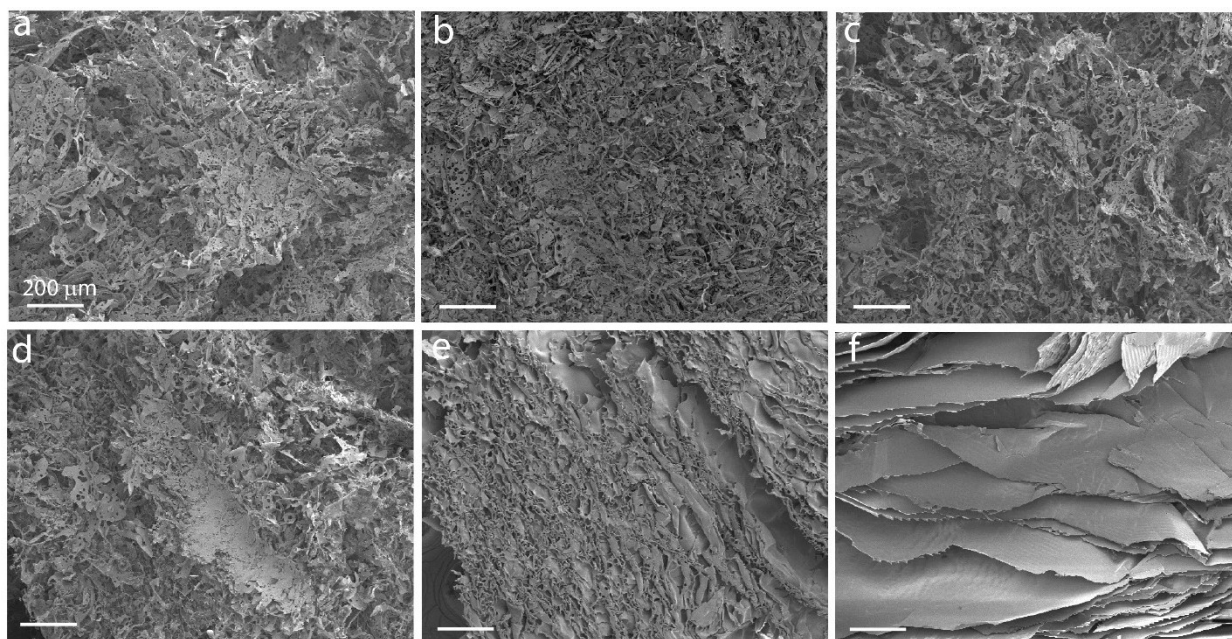
Supplementary Figure 39. The morphology of lyophilized powder of various constructs. a) M-B$_1$-ELP; b) M-B$_2$-ELP; c) M-B$_3$-ELP; d) B$_3$-ELP (as a representative example of non myristoylated construct); e) M-ELP and f) ELP. HPLC was used to purify constructs shown in (a-e). ELP was purified using three rounds of ITC.

22. Aggregation above T$_c$

For M-B$_2$-ELP, the onset of T$_c$ (defined as the critical temperature corresponding to sudden decrease in the turbidity) depends on the nominal concentration of the protein in solution (Figure 2e). For example, at 100 μM, T$_c$ is approximately 45 °C; at 50 μM, T$_c$ is approximately 50 °C. We do not observe T$_c$ in solution containing 25 μM below 50 °C (The upper limit in our experiments). In the case of M-B$_3$-ELP, T$_c$ does not show the same dependence on the initial concentration (i.e. at all concentrations T$_c$ appears to be ~ 50 °C (Figure 2h).

This observation is consistent with a mechanism discussed in the paper. We propose that ELP chains are responsible for the stabilization of aggregates during stage 1 and to some extent in stage 2. The last stage of self-assembly manifested at higher temperatures ($T > T_c$), where the repulsion between the ELP coronas is reduced due to further dehydration, which results in a decrease in the core-core(PA-domain) distances inside the coacervates. At some point, it is possible that the cores are connected (non-covalently cross-linked) through a dynamic rearrangement (i.e. the formation of bundle fibers in M-B_2-ELP). If the cores are held together by very strong forces, as appears to be the case in M-B_3-ELP, this dynamic rearrangement may not occur in the window of opportunity before non-specific aggregation of the ELP chains, resulting in the formation of ill-defined aggregates.

Dynamic of core-core supramolecular cross-linking will depend on the strength of interactions holding these cores together, and the concentration of self-assembly intermediates. In the case of M-B_2-ELP with weaker core interaction (lower propensity to form β-sheets), increasing the concentration of aggregates in solution is expected to decrease T_c.

Additionally, one can predict that increasing the size of the ELP length (i.e. protective corona) should increase T_c. We have conducted this simple experiment, using M-B_2-ELP$_{20}$ and M-B_2-ELP$_{60}$ (subscript denotes the number of pentapeptide repeats). As shown in Supplementary Figure 40, our prediction is consistent with the result of turbidity experiments. T_c for M-B_2-ELP$_{20}$ at 100 μM is lowered to ~ 40 °C (Supplementary Figure 40a) and no critical aggregation is observed for M-B_2-ELP$_{60}$ at the same concentration up to 50 °C (Supplementary Figure 40b). The inset is an optical image of the cuvette immediately at the end of the experiment. M-B_2-ELP$_{20}$ formed condensed aggregates (marked with an arrow), similar to M-B_2-ELP discussed in the paper, while M-B_2-ELP$_{60}$ is homogeneously turbid with no observable macroaggregate. M-B_2-ELP$_{20}$ aggregates remained stable below T_t while M-B_2-ELP$_{60}$ solution turned clear below T_t.
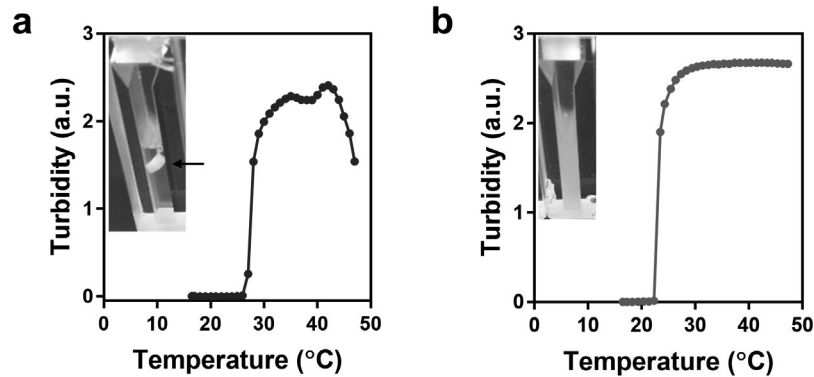
Supplementary Figure 40. a) Temperature-programmed turbidimetry assay of M-B$_2$-ELP$_{20}$. b) Temperature-programmed turbidimetry assay of M-B$_2$-ELP$_{60}$. The inset in each case is an optical image of the cuvette immediately after the end of the experiments. As shown in the figure, T$_c$ is dependent on the ELP domain length.

23. References

1.   Maurer-Stroh, S., Eisenhaber, B. & Eisenhaber, F. N-terminal N-myristoylation of proteins: prediction of substrate proteins from amino acid sequence. *J. Mol. Biol.* **317,** 541–557 (2002).

2.   Zhang, J. *et al.* Self-assembly of a peptide amphiphile based on hydrolysed Bombyx mori silk fibroin. *Chem. Commun. (Camb).* **47,** 10296–8 (2011).

3.   Lee, O.-S., Stupp, S. I. & Schatz, G. C. Atomistic molecular dynamics simulations of peptide amphiphile self-assembly into cylindrical nanofibers. *J. Am. Chem. Soc.* **133,** 3677–3683 (2011).

4.   Cui, H., Cheetham, A. G., Pashuck, E. T. & Stupp, S. I. Amino acid sequence in constitutionally isomeric tetrapeptide amphiphiles dictates architecture of one-dimensional nanostructures. *J. Am. Chem. Soc.* **136,** 12461–12468 (2014).

5.   Minor, D. L. & Kim, P. S. Measurement of the [beta]-sheet-forming propensities of amino acids. *Nature* **367,** 660–663 (1994).

6.   Smith, C. K., Withka, J. M. & Regan, L. A thermodynamic scale for the beta-sheet forming tendencies of the amino acids. *Biochemistry* **33,** 5510–7 (1994).

7.   Minor, D. L. & Kim, P. S. Context is a major determinant of beta-sheet propensity. *Nature* **371,** 264–267 (1994).

8.   McDaniel, J. R., Radford, D. C. & Chilkoti, A. A unified model for de novo design of

elastin-like polypeptides with tunable inverse transition temperatures. *Biomacromolecules* **14,** 2866–2872 (2013).

9. McDaniel, J. R., MacKay, J. A., Quiroz, F. G. & Chilkoti, A. Recursive directional ligation by plasmid reconstruction allows rapid and seamless cloning of oligomeric genes. *Biomacromolecules* **11,** 944–952 (2010).

10. Coin, I., Beyermann, M. & Bienert, M. Solid-phase peptide synthesis: from standard procedures to the synthesis of difficult sequences. *Nat. Protoc.* **2,** 3247–56 (2007).

11. Greenfield, N. J. Using circular dichroism spectra to estimate protein secondary structure. *Nat. Protoc.* **1,** 2876–2890 (2006).

12. Nuhn, H. & Klok, H. A. Secondary structure formation and LCST behavior of short elastin-like peptides. *Biomacromolecules* **9,** 2755–2763 (2008).

13. Paramonov, S. E., Jun, H. W. & Hartgerink, J. D. Self-assembly of peptide-amphiphile nanofibers: The roles of hydrogen bonding and amphiphilic packing. *J. Am. Chem. Soc.* **128,** 7291–7298 (2006).

14. Kelly, S. M., Jess, T. J. & Price, N. C. How to study proteins by circular dichroism. *Biochimica et Biophysica Acta - Proteins and Proteomics* **1751,** 119–139 (2005).

15. Serrano, V., Liu, W. & Franzen, S. An infrared spectroscopic study of the conformational transition of elastin-like polypeptides. *Biophys. J.* **93,** 2429–2435 (2007).

16. Jiang, H., Guler, M. O. & Stupp, S. I. The internal structure of self-assembled peptide amphiphiles nanofibers. *Soft Matter* **3,** 454 (2007).

17. Ciofani, G. *et al.* Recombinant Human Elastin-like Magnetic Microparticles for Drug Delivery and Targeting. *Macromol. Biosci.* **14,** 632–642 (2014).

18. Lin, S.-Y., Hsieh, T.-F. & Wei, Y.-S. pH- and thermal-dependent conformational transition of PGAIPG, a repeated hexapeptide sequence from tropoelastin. *Peptides* **26,** 543–549 (2005).

19. Stsiapura, V. I. *et al.* Thioflavin T as a Molecular Rotor: Fluorescent Properties of Thioflavin T in Solvents with Different Viscosity. *J. Phys. Chem. B* **112,** 15893–15902 (2008).

20. Sulatskaya, A. I., Maskevich, A. A., Kuznetsova, I. M., Uversky, V. N. & Turoverov, K. K. Fluorescence Quantum Yield of Thioflavin T in Rigid Isotropic Solution and Incorporated into the Amyloid Fibrils. *PLoS One* **5,** e15385 (2010).

21. Muiznieks, L. D. *et al.* Modulated growth, stability and interactions of liquid-like coacervate assemblies of elastin. *Matrix Biol.* **36,** 39–50 (2014).

22. Hayashi, S. & Okada, Y. Ultrafast superresolution fluorescence imaging with spinning disk confocal microscope optics. *Mol. Biol. Cell* **26,** 1743–1751 (2015).

23. Simon, J. R., Carroll, N. J., Rubinstein, M., Chilkoti, A. & Lopez, G. P. Programming molecular self-assembly of intrinsically disordered proteins containing sequences of low complexity. *Nat. Chem.* **9,** 509–515 (2017).

24. Mcdaniel, J. R. *et al.* Noncanonical self-assembly of highly asymmetric genetically encoded polypeptide amphiphiles into cylindrical micelles. *Nano Lett.* **14,** 6590–6598 (2014).

25. Derjaguin, B. V., Muller, V. M. & Toporov, Y. P. Effect of contact deformations on the adhesion of particles. *J. Colloid Interface Sci.* **53,** 314–326 (1975).